frontiers | Frontiers in Earth Science

TYPE Original Research
PUBLISHED 08 January 2024
DOI 10.3389/feart.2023.1295271

OPEN ACCESS

EDITED BY
Claudia Belviso,
National Research Council (CNR), Italy

REVIEWED BY
Eun Young Lee,
University of Vienna, Austria
Sherif Farouk,
Egyptian Petroleum Research Institute, Egypt

*CORRESPONDENCE
Khaled G. Elmaadawy,
kelmaadawy@yahoo.com
Mostafa R. Abukhadra,
abukhadra89@science.bsu.edu.eg
Stefano Bellucci,
stefano.bellucci@lnf.infn.it

RECEIVED 15 September 2023
ACCEPTED 18 December 2023
PUBLISHED 08 January 2024

CITATION
Elmaadawy KG, Bayan MF, Gad M, Szűcs P, Eid MH, Abukhadra MR, El-Sherbeeny AM, Bellucci S and Abdelmaksoud AS (2024), The impact of Oligo-Miocene basaltic intrusions on the petroleum system in Gulf of Suez rift basin, Egypt: new insights into thermal maturity and reservoir quality. *Front. Earth Sci.* 11:1295271. doi: 10.3389/feart.2023.1295271

The impact of Oligo-Miocene basaltic intrusions on the petroleum system in Gulf of Suez rift basin, Egypt: new insights into thermal maturity and reservoir quality

Khaled G. Elmaadawy[1]*, Mahmoud F. Bayan[1], Mohamed Gad[2], Péter Szűcs[3], Mohamed Hamdy Eid[4,3], Mostafa R. Abukhadra[5,4]*, Ahmed M. El-Sherbeeny[6], Stefano Bellucci[7]* and Ashraf S. Abdelmaksoud[1]

[1]Geology Department, Faculty of Science, Menoufia University, Shiben El Kom, Egypt, [2]Evaluation of Natural Resources Department, Environmental Studies and Research Institute (ESRI), University of Sadat City, Sadat City, Egypt, [3]Faculty of Earth Science, Institute of Environmental Management, University of Miskolc, Miskolc, Hungary, [4]Geology Department, Faculty of Science, Beni-Suef University, Beni-Suef, Egypt, [5]Materials Technologies and Their Applications Lab, Geology Department, Faculty of Science, Beni-Suef University, Beni-Suef, Egypt, [6]Industrial Engineering Department, College of Engineering, King Saud University, Riyadh, Saudi Arabia, [7]INFN, Laboratori Nazionali di Frascati, Frascati, Italy

In recent years, the petroleum industry has prioritized the exploration of new and unconventional petroleum reservoirs. As a result, this study assessed the significance of basaltic intrusions from two key aspects: their impact on the thermal maturity of pre-rift source rocks and their potentiality as reservoirs. The present study attempts to integrate surface field investigations of basaltic dykes in Wadi Nukhul and Wadi Matulla as surface analogs with petroleum system modeling of pre-rift source rocks containing subsurface basaltic intrusions in the Abu Rudeis-Sidri field. Therefore, the fracture networks were observed in Wadi Nukhul and Wadi Matulla, suggesting that both the basaltic dykes and host rocks have interconnected fractures, which is critical for a high-quality reservoir of the dykes and efficient oil expulsion. As a result, the analysis of burial history, temperature, maturity, generation, transformation ratio, and expelled oil quantity revealed a significantly high value for basaltic intrusions. Moreover, the Abu Rudeis-Sidri field had a good petroleum system with thermally mature source rocks by basaltic intrusions. Furthermore, the fractured basaltic intrusions presented a high-quality oil reservoir well-sealed by the thick Rudeis Formation. Oil production has doubled since the discovery of this reservoir. This study introduces a novel approach to understanding the distribution pattern of basaltic intrusions in subsurface and surface analogs, which can serve as a model for exploring new potential unconventional basaltic reservoirs in the Gulf of Suez rift basin.

KEYWORDS

basaltic intrusion reservoirs, Wadi Nukhul basaltic dyke, Wadi Matulla basaltic dyke, pre-rift source rocks, Abu Rudeis-Sidri field, Gulf of Suez rift basin

1 Introduction

Organic matter maturity and hydrocarbon potential in sedimentary basins are significantly influenced by the thickness and timing of the emplacement of igneous intrusions (Sydnes et al., 2018). During the cooling of the igneous intrusion, the heat transferring is experienced to the thickness of the thermally altered rocks and the lithology type (Wang et al., 2007). The thick sill

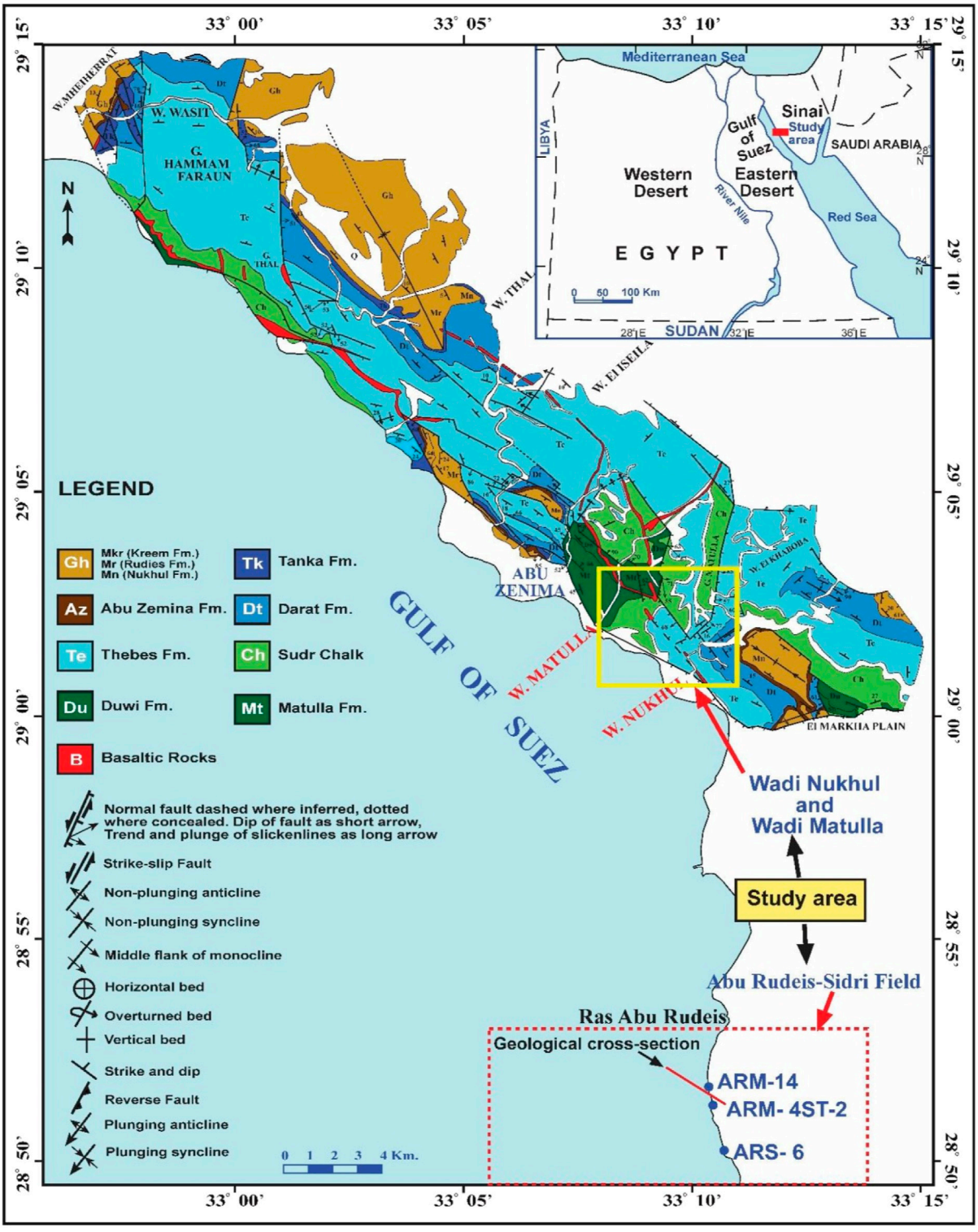

FIGURE 1
Location map of the study area showing Wadi Nukhul and Wadi Matulla in the western side of Sinai, highlighted in the yellow square, with accompanying geological map (Moustafa, 2004). The Abu Rudeis-Sidri Field on the eastern side of the Gulf of Suez is also shown in a red square.

intrusions close to the source rocks at great depth increase the thermal maturity history more than the thin igneous intrusions (Hubred, 2006). The main factors necessary for the conversion of organic matter into hydrocarbons are thermobaric conditions, the type and composition of organic matter, and the burial history of the sedimentary basin (Palumbo et al., 1999; Roberts et al., 2007; Grobe et al., 2015; Simandl et al., 2015). The thermal history and maturity of the sedimentary basins were influenced by the igneous intrusions (Galushkin, 1997; Othman et al., 2001; Aarnes et al., 2011; 2010; Wang et al., 2013; 2012; Peace et al., 2017; Schofield et al., 2017). Due to igneous intrusions, the temperature rises upon contact with the host rocks and decreases over time, leading to an increase in the transformation ratio (Fjeldskaar et al., 2008). Despite the relatively low total organic content (TOC) in the source rocks, gas generation within the host rock can be significant due to sill intrusions (Aarnes et al., 2015). The vitrinite reflectance increases at contact with or near the igneous intrusions and decreases far away (Stewart et al., 2005). In Svalbard, Norway, the organic matter of the Triassic section was strongly thermally altered by the Early Cretaceous dolerite intrusions (Brekke et al., 2014). In rifted margin basins, the interplay between the igneous intrusion and the host rocks led to an oil window in immature source rocks and a gas window in mature source rocks (Muirhead et al., 2017). The mafic igneous intrusions increase the maturity level of the immature source rocks to an oil window (Reeckmann and Mebberson, 1984; Muirhead et al., 2020). In southwest Colombia, dykes and sills of gabbro raised hydrocarbon generation and expulsion to the gas window (Vásquez et al., 2009). Based on seismic interpretation, the direction of intrusion flow was controlled by the basin's main structure trend, forming numerous sub basins (Schofield et al., 2017).

Many countries, such as the United States, eastern China, and Argentina, have igneous intrusion reservoirs (Schutter, 2003a; Wu et al., 2006; Delpino and Bermúdez, 2009; Witte et al., 2012). The igneous reservoirs are characterized by types of primary vesicular porosity, secondary porosity with hydrothermal alteration, and fracture porosity (Schutter, 2003a). Vesicular basalt has high porosity ranging from 30% to 50%, attributed to fracture porosity experienced due to tectonic stress, thermal alteration, and dissolution (Chen et al., 1999). The primary factors controlling the petrophysical properties of volcanic rocks, including basaltic dykes, are lithology and degree of alteration (Lee et al., 2021). The volcanic reservoir is characterized primarily by fracture porosity associated with pores formed by dissolved phenocrysts and matrix and gas pores connected by fractures (Chen et al., 2016).

The study area is located in the eastern portion of the Gulf of Suez and the western side of Sinai between 29° 00` and 28° 50` N latitude and 32° 70` and 33° 15` E longitude (Figure 1). The area's northern boundary coincides with Wadi Mheiherrat, and the southern border is Abu Rudeis. The extension of Wadi Mheiherrat delimits the eastern side of the study area, including Wadi Thal, Wadi El Iseila, and Wadi El Khaboba, from the northwest to the southeast in a line parallel to the shoreline of the Gulf of Suez. The Wadi Nukhul and Wadi Matulla locations and the Abu Rudeis-Sidri Field both contain basaltic intrusions that intruded pre-rift source rocks. They have the same lithostratigraphic sequence. Furthermore, the Abu Rudeis-Sidri Field has already successfully produced oil from a basaltic intrusion reservoir. The Wadi Nukhul and Wadi Matulla outcrops represent the closest surface exposures of these types of basaltic intrusions to the subsurface Abu Rudeis-Sidri Field. Notably, wells penetrating the basaltic intrusions in the Abu Rudeis-Sidri Field exhibited a doubling of oil production rates, demonstrating the reservoir potential. Therefore, the Wadi Nukhul and Wadi Matulla basaltic intrusions can serve as useful analogues to assess the reservoir quality and hydrocarbon potential of the intrusions in the Abu Rudeis-Sidri Field.

Dykes, sills, and flows mark the early rift of the Gulf of Suez in the Oligo-Miocene (Patton et al., 1994). A few late pre-rift to early syn-rift basic dykes are distributed along the Gulf of Suez, including the study area (Kazmin and Byakov, 2000; Bosworth and McClay, 2001). The dykes in the Abu Zenima and Hammam Faraoun areas have thicknesses ranging from 10 m to 30 m, with the dykes nearly vertical, and the hypothesis that the dyke emplacement is in tension fissures is correct because there is no indication of displacement on the sides of the dykes (Ragab and El-Kaliouby, 1992). In the study area, dykes, sills, and flows are 22–24 Ma old (Steen, 1982; Mousa, 1987), and these volcanic basalts of the Early Miocene are the first evidence of rifting recorded. The abundant orientation of the dykes of early Miocene age in the area is NW-SE, subparallel to the rift trend; under the tensional stresses in the area in the early stage of rift opening, these dykes were intruded (Moustafa, 1993).

Only a limited number of published studies have focused on basaltic intrusions and their impact on hydrocarbon potential in the Gulf of Suez petroleum province. Sharib et al. (2019) conducted a study on the outcrop of a basaltic dyke in Wadi Matulla, examining its thermal influence on the maturity of the pre-rift source rock (PRSR) of the Sudr Formation (Sharib et al., 2019). Abd El-Gawad et al. (2022), Abd El-Gawad et al. (2021) investigated the basaltic intrusions as an oil reservoir in the Abu Rudeis-Sidri field and studied their distribution style.

Therefore, this study aims to (i) investigate the Oligo-Miocene basaltic intrusions (OMBIs) in Wadi Nukhul and Wadi Matulla as surface analogs of the subsurface basaltic intrusion dyke's reservoir and their thermal influence on the maturity of source rocks and expulsion of hydrocarbons; (ii) analyze the fracture network in Nukhul and Matulla dykes, comparing them with fractures in subsurface basaltic intrusions in Abu-Rudeis Sidri field and fractures in Thebes and Matulla formations; (iii) examine the influence of basaltic intrusions on the pre-rift petroleum system, with a specific focus on their effects on charging and reservoir potential; (iv) study the distribution pattern of basaltic intrusions and their effects on source rock maturity of the pre-rift source rocks (PRSRs) and reservoir quality.

2 Geologic and tectonic setting

The exposed rocks of the study area range in age from Coniacian-Santonian to Middle Miocene, including pre-rift and syn-rift sequences (Figure 2A). The pre-rift sequence is represented by formations from Matulla at the base to Thebes at the top, and the syn-rift sequence is represented by Nukhul, Rudeis and Kareem formations. Matulla Formation is composed of sandstone, shale, claystone, and calcareous sandstone with dolomitic limestone (Zalat et al., 2012), and Duwi Formation

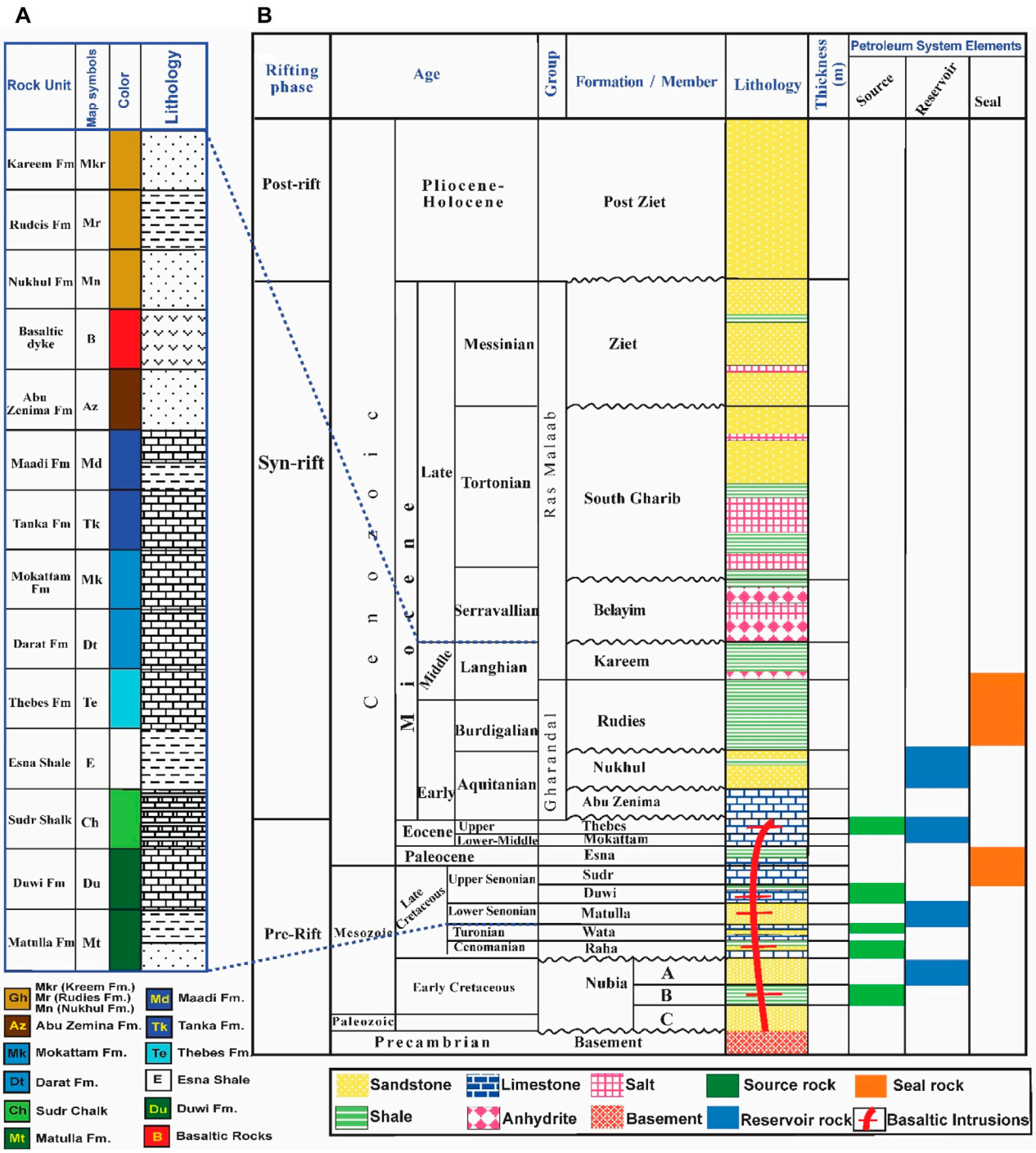

FIGURE 2
(A) Surface lithostratigraphic sequence for the eastern side of the Gulf of Suez, including Wadi Nukhul and Wadi Matulla adapted from Moustafa (2004); **(B)** subsurface lithostratigraphic column of Abu Rudeis-Sidri field (modified after Elmaadawy et al., 2021).

consists of clays, sandstones, and limestones from shallow marine conditions (Youssef, 1949; 1957). Sudr Chalk is composed of hard white chalk with chalky limestone (Ghorab, 1961), and Esna Shale is composed of greenish shale overlying the Sudr Chalk with sharp contact (Said, 1960). The Thebes Formation consists of gray to white limestone with chert bands (Moustafa, 2004). The Darat Formation consists of shale and marl with thin limestone beds and the Mokattam Formation composed of yellowish-white limestone (Bosworth and McClay, 2001; Moustafa, 2004). The Tanka Formation comprises chalky and argillaceous limestone intercalated with thin shale beds (Abuseda et al., 2015). The Maadi Formation is composed of shale intercalated with limestone beds (Said, 1962). The Abu Zenima Formation is made up of white and red sandstone and siltstone, as well as basalt pebbles

and conglomerate, and is capped by basaltic flow (Plaziat et al., 1998). The rifting of the Gulf of Suez profoundly impacted Upper Oligocene and Miocene deposits in western and central Sinai, such as in the Wadi Baba, Wadi Gharandal and Nukhul–Sudr areas (Hewaidy et al., 2012; 2013; Ayyad et al., 2023). The Lower Miocene Nukhul sandstones, which produce oil in the Abu Rudeis-Sidri Field, are characterized by four systems tracts that experienced sea level changes during the rifting phase of the Gulf of Suez (Hewaidy et al., 2012; Abu Shama et al., 2023; Farouk et al., 2023). Nukhul Formation consists of sandstones, conglomerates, and marl with cross-bedded sandstones (Scott and Govean, 1985). The Rudeis Formation is composed of fine-grained sandstone with marl at the lower part graded into glauconitic and fossiliferous coarse sandstone at the top (Garfunkel et al., 1974; Beleity, 1982). The stratigraphic section is topped by the Kareem Formation, consisting of sandstones, shales, and carbonates with anhydrites, which rests unconformably on the Rudeis Formation (Hughes et al., 1992; El Nady and Mohamed, 2016). The subsurface lithostratigraphic section of the Abu Rudeis-Sidri field is composed of three major sequences of pre-rift, syn-rift, and post-rift from base to top (Figure 2B). In the Gulf of Suez rift basin, source rocks are distributed across both pre-rift deposits (including the Duwi, Esna, Sudr and Thebes formations) and syn-rift deposits (including the Rudeis and Kareem formations). The pre-rift source rocks were deposited under anoxic conditions and contain marine organic matter of kerogen types I and (Barakat, 1982; Salah, 1992; Alsharhan and Salah, 1994; 1997; Wever, 1999; Alsharhan, 2003; Younes and Philp, 2005; El Nady and Mohamed, 2016; Elmaadawy et al., 2021).

The rift faulting that started in the Oligocene and continued into post-Miocene times resulted from regional extensional stress more or less perpendicular to the rift axis (Robson, 1971; Chenet et al., 1987). The age of the Red Sea opening ranged from the late Oligocene to the Middle Miocene, during which the Red Sea rift developed through the mixing of normal faults and dykes in the late Oligocene or early Miocene (Coleman and Billington, 1979). The Gulf of Suez rift with the primary trend (N30W) and the Gulf of Aqaba with the primary trend (N25E) are the two branches of the Red Sea rift (Badawy and Abdel-Fattah, 2006).

The Suez rift was opening perpendicular to a NE-SW extension in the early Miocene, which was also the opening of the northern Red Sea at the time, with the Suez Gulf reaching its maximum width in Miocene time (Mart and Hall, 1984). In central Sinai, near Abu Zenima and Hammam Faraoun, volcanic rocks spread as dolerite dykes, sills, and flows, in which these volcanic rocks intruded rocks up to the Middle Eocene (Meneisy, 1990; Said, 1990). The basement structures strongly influenced the evolution of the Gulf of Suez rift through four Wadi systems opening into the Gulf of Suez. They also played a crucial role in shaping the geological features of the area. These Wadi systems include the following: Wadi Nukhul, running from the west shoreline of the Gulf of Suez to the east; Wadi Matulla, running from southwest to northeast; Wadi Tayiba, running from north to south; Wadi Wasit, running from west to east (Bosworth et al., 2005).

The Red Sea rift system including the Gulf of Suez rift was associated with the volcanism of basaltic intrusions (Bosworth and Stockli, 2016). In Egypt, this Cenozoic volcanism has many forms including basaltic dykes, basaltic flows and cones of basaltic cones. The basalts alore distributed from Libyan Plateau in the west to Sinai in the east related to the NW-SE faults (Baldridge et al., 1991; Abdel Aal, 1998; Endress et al., 2011). Basaltic dykes in Wadi Nukhul and Wadi Matulla range from olivine dolerites and olivine-bearing basalts to vitrophyric, texturally heterogeneous basalts and crystal lithic tuffs. The transitional tholeiitic basalts display low compatible element concentrations and an enrichment of the whole spectrum of the incompatible elements. Major, trace and Rare Earth Element data suggest that the melts formed by 5% melting of mantle peridotite at the spinel–garnet transition zone (80–90 km depth), in the presence of 2%–4% residual garnet. During the melt ascent, the fractionating phases were olivine, clinopyroxene and, to a lesser extent, plagioclase (Shallaly et al., 2013). The basaltic dyke is vitrophyric composed of subhedral to euhedral phenocrysts of sericitized plagioclase fresh to partially altered olivine and few clinopyroxene crystals floating in a cryptocrystalline to glassy ground mass. Accessory phases include Fe-oxides and apatite (Sharib et al., 2019).

The major trends of normal faults in the study area are NW and NNW, parallel to the Gulf of Suez trend (Hegazi, 1995). The NW-oriented fault in the Hammam Faroun area exits before the Neogene opening of the Suez rift. In the Oligocene-Miocene, the NW-oriented pre-rift fault was revitalized as diagonal-slip faults. NW-oriented faults are normal, right lateral, or left lateral diagonal slips (Khedr, 2003). The NNE normal faulting regime was related to the Gulf of Aqaba tectonics, which prevailed during the Late Oligocene–Early Miocene with left lateral slip movement (Hegazi, 1995). The NE fault populations are of extensional origin and rejuvenated by left-lateral strike-slip faults in many localities (Seleem and Khalifa, 2006).

3 Data and methodology

3.1 Surface field study

3.1.1 Lineations

The orientations of all lineaments were extracted based on the Landsat image through automatic detection using PCI Geomatica, 2017 software (Geomatica, 2017) for the area between 29° 00` and 29° 14` N latitude and 32° 70` and 33° 15` E longitude. Additionally, ArcMap v10.4.1 was used to edit and calculate the coordinates for extracting lineaments. Moreover, RockWorks 16 software was used to draw a rose diagram and to interpret the lineaments, including fractures, faults, dykes, and shear zones.

3.1.2 Fracture pattern quantification

Quantification of fracture patterns in 2D based on field photography was determined using FracPaQ software of Healy et al. (Healy et al., 2017). The fractures were traced and processed to develop fracture trace maps used to study fracture properties such as orientations, lengths, permeability, connectivity, intensity, and density (Dershowitz and Herda, 1992). The fracture density (P20) is defined as the number of fractures per unit area (m^{-2}), while the fracture intensity (P21) is defined as the sum of all fracture lengths in a given area (thus, $m/m^2 = m^{-1}$). The connectivity and the 2D-permeability ellipse plots were linked to research on fluid flow in

10.3389/feart.2023.1295271

TABLE 1 The input data used to construct the burial history model for well ARS-6.

Formation/ events	Age (Ma)	Eroded thickness (m)	Lithology %				Formation tops (m)	Formation thickness (m)
			Sandstone	Shale	Evaporites	Limestone		
Erosion	0.8	20						
Post Zeit Fm	5.3		93	7	—	—	4.0	1428.0
Erosion	5.5	350						
Zeit	7.2		15	43	42	—	1432.0	130.0
South Gharib Fm	11.8		—	11	89	—	1562.0	370.0
Belayim Fm	13.6		—	37	63	—	1932.0	233.0
Kareem Fm	15.8		10	90	—	—	2165.0	78.0
Rudeis Fm	16		3	97	—	—	2243.0	359.0
Hiatus	20							
Nukhul Fm	22		25	25	—	50	2602.0	73.0
Hiatus	24							
Abu Zenima Fm	28		—	49	—	49	2675.0	35.0
Erosion	46	5						
Thebes Fm	50.6		—	—	—	100	2710.0	287.0
Esna Fm	62.8		—	58	—	42	2997.0	33.0
Duwi Fm	83		—	—	—	100	3030.0	84.0
Erosion	84.5	10						
Matulla Fm	88.5		63	17	—	20	3114.0	119.0
Erosion	89	35						
Wata Fm	93		11	24	—	65	3233.0	100.0
Raha Fm	95.5		21	37	—	42	3333.0	94.0
Erosion Fm	245	10						
Nubia Fm	540		45	55	—	—	3427.0	708.0

S.S., sandstones; Sh. shales; Eva. evaporites; L.S., limestones.

rock fracture networks (Healy et al., 2017). The connectivity diagram was constructed depending on nodes as the isolated ends of traces (I), branch points, splays, or abutments (Y), and cross-cutting intersections (X). These nodes are the three vertices of the connectivity ternary plot of the fracture network. In this diagram, more connected networks plot toward the lower Y-X side, while less connected networks plot toward the apex (I) (Manzocchi, 2002). The outputs were represented in fracture networks, fracture density (P20) map, fracture intensity (P21) map, connectivity, and permeability for fracture networks. Thin sections were prepared for basalt dykes from Wadi Nukhul and Wadi Matulla to investigate pore and fracture types, lengths and widths, and their relation with reservoir quality.

3.2 Subsurface study for basin and petroleum systems modeling

To reconstruct the models, the input data required are the initial ages of the formations, intervals of hiatuses and erosions, lithology types along with their respective percentages for each formation, and the formation tops with their thicknesses for wells ARS-6 and ARM-4 (Table 1 and Supplementary Table S1). The modeling process involves various aspects such as burial, thermal history, maturity, generation, and expulsion histories of the basin and petroleum systems. For maturity modeling, we utilized the model proposed by Suzuki (1993). For generation modeling, we relied on the kinetic model of Pepper and Corvi (1995). The thermal maturity data were validated for the wells of the Abu Rudeis-Sidri Field by Elmaadawy et al. (2021).

4 Results

4.1 Lineaments

The identified lineaments were 1533, including fractures, faults, dykes, and shear zones, and based on their strikes, they were subdivided into six trends: NW, NNW, NNE, NE, WNW, and

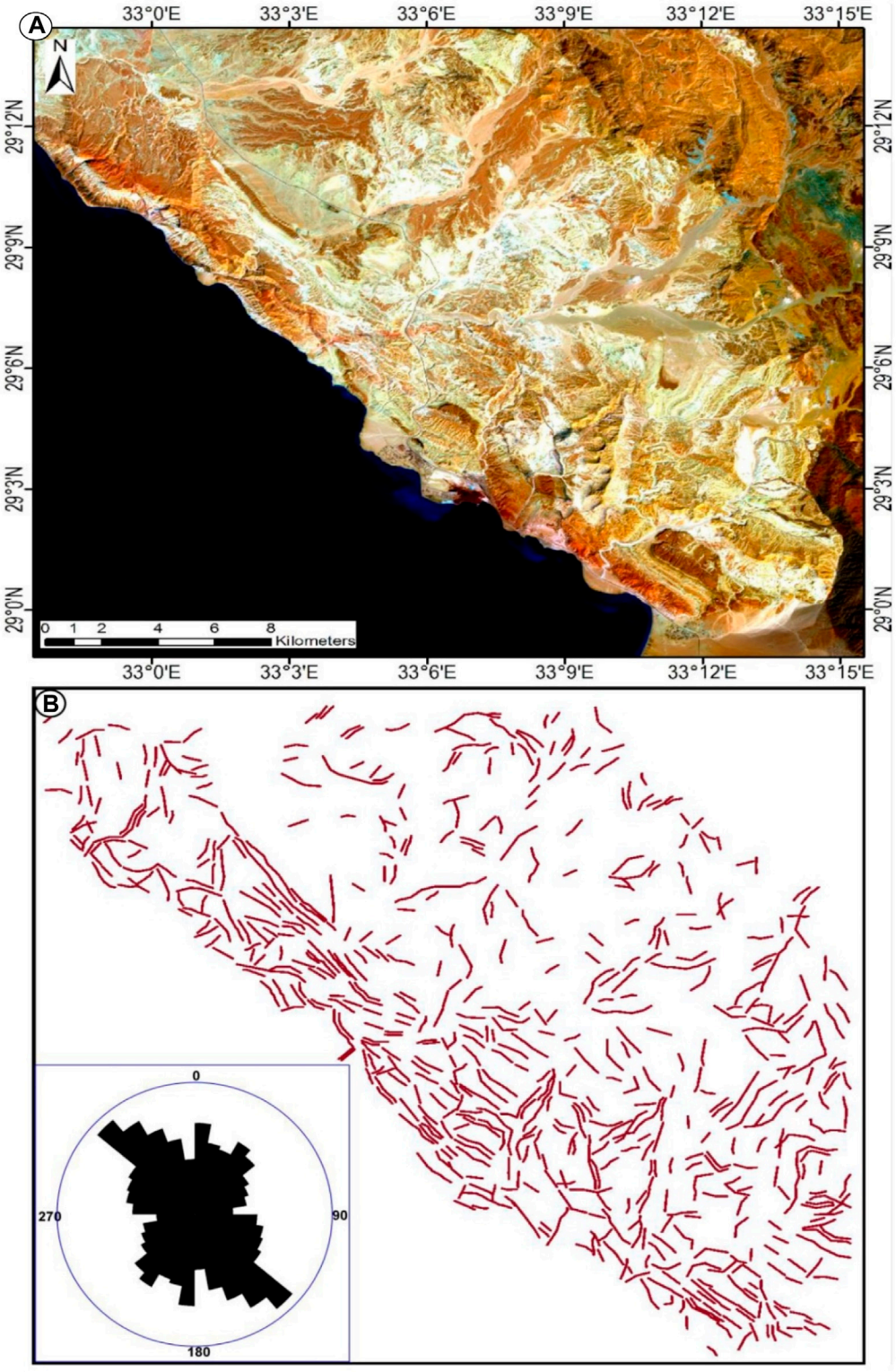

FIGURE 3
(A) Landsat ETM image of the whole area; **(B)** lineaments network with rose diagram showing the trends of lineaments.

ENE (Figure 3). The dominant trends were NW and NNW, including normal faults that parallel the Gulf of Suez rift trend. Normal faults with trends NE and NNE attributed to Gulf of Aqaba tectonics during the Oligo-Miocene. The minor trends that have little effect on the tectonic evolution of the area were in the WNW and ENE directions.

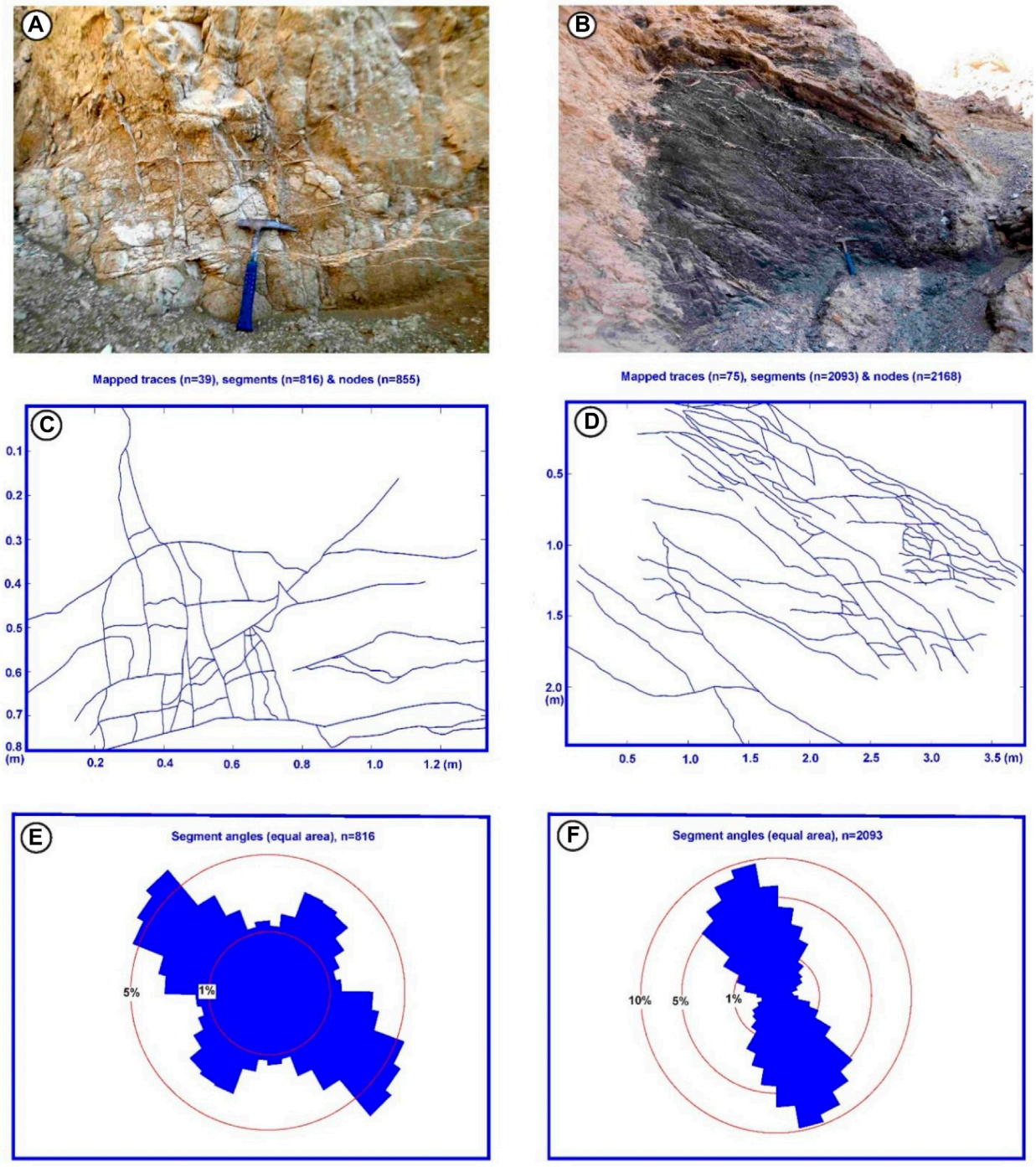

FIGURE 4
Two fractured networks observed in Wadi Nukhul. **(A)** Outcrop of a fractured limestone network, photograph looking NE; **(B)** outcrop of a fractured black limestone network, photograph looking SW; **(C)** fracture trace map of fractured limestone of the photograph shown in **(A)**; **(D)** fracture trace map of a fractured black shale photograph shown in **(B)**; **(E)** angles of fracture segments from a limestone network and distribution of fracture orientations in the rose diagram; **(F)** angles of fracture segments from a black shale network and distribution of fracture orientations in the rose diagram.

4.2 Fracture networks

Four locations were selected for constructing the fracture networks, including two in Wadi Nukhul and two in Wadi Matulla. In Wadi Nukhul, fracture networks were constructed for two locations in contact with the basaltic dyke. The first location represents the limestone on the eastern side of the dyke, and the second represents the black limestone on the western side (Figure 4). The rose plots of the fracture network on limestone revealed a two-abundance orientation of the fracture population in the NW and

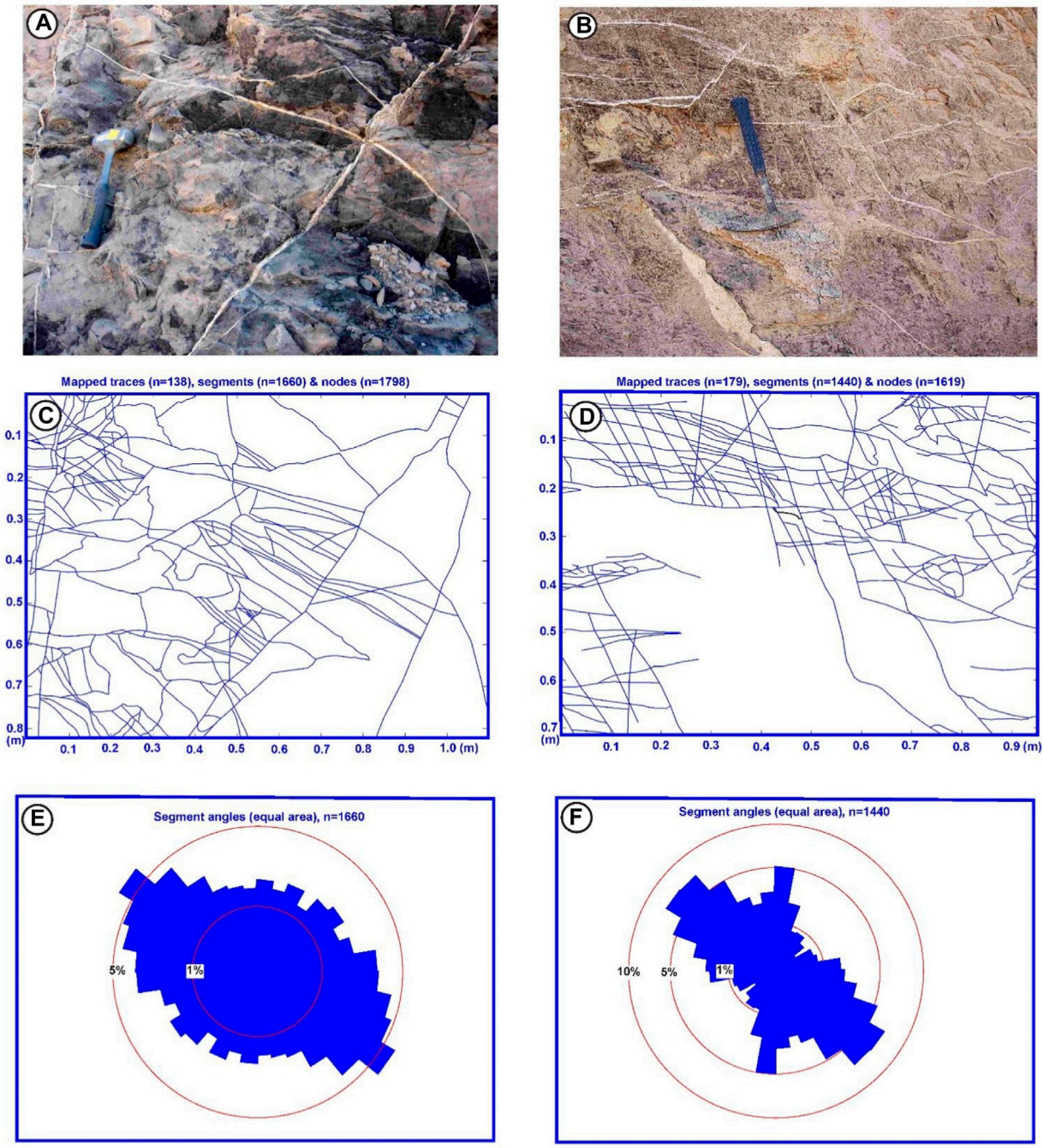

FIGURE 5
Two fractured networks observed in Wadi Matulla. **(A)** Outcrop of a fractured basaltic dyke, photograph looking south; **(B)** outcrop of a fractured shale network, photograph looking SE; **(C)** fracture trace map of the fractured dyke of the photograph shown in **(A)**; **(D)** fracture trace map of a fractured shale photograph shown in **(B)**; **(E)** angles of fracture segments from a basaltic dyke network and distribution of fracture orientations in the rose diagram; **(F)** angles of fracture segments from a shale network and distribution of fracture orientations in the rose diagram.

NE, respectively (Figure 4E). The direction of the fracture population of the black limestone was NNW (Figure 4F). In Wadi Matulla, fracture segment angles were plotted: the first fracture network of the Matulla basaltic dyke with two standard orientations in the NW and NE (Figure 5E) and the abundance orientation of the second fracture observed on shale in the NW and NNE (Figure 5F).

4.3 Fracture density and intensity maps

The density map of the limestone fracture network in Wadi Nukhul (Figure 6A) revealed two or more distinct clusters of high density (i.e., many fractures per square meter), with the highest values of density clusters focused in the center and extending in the NW direction. The fracture intensity map of the limestone

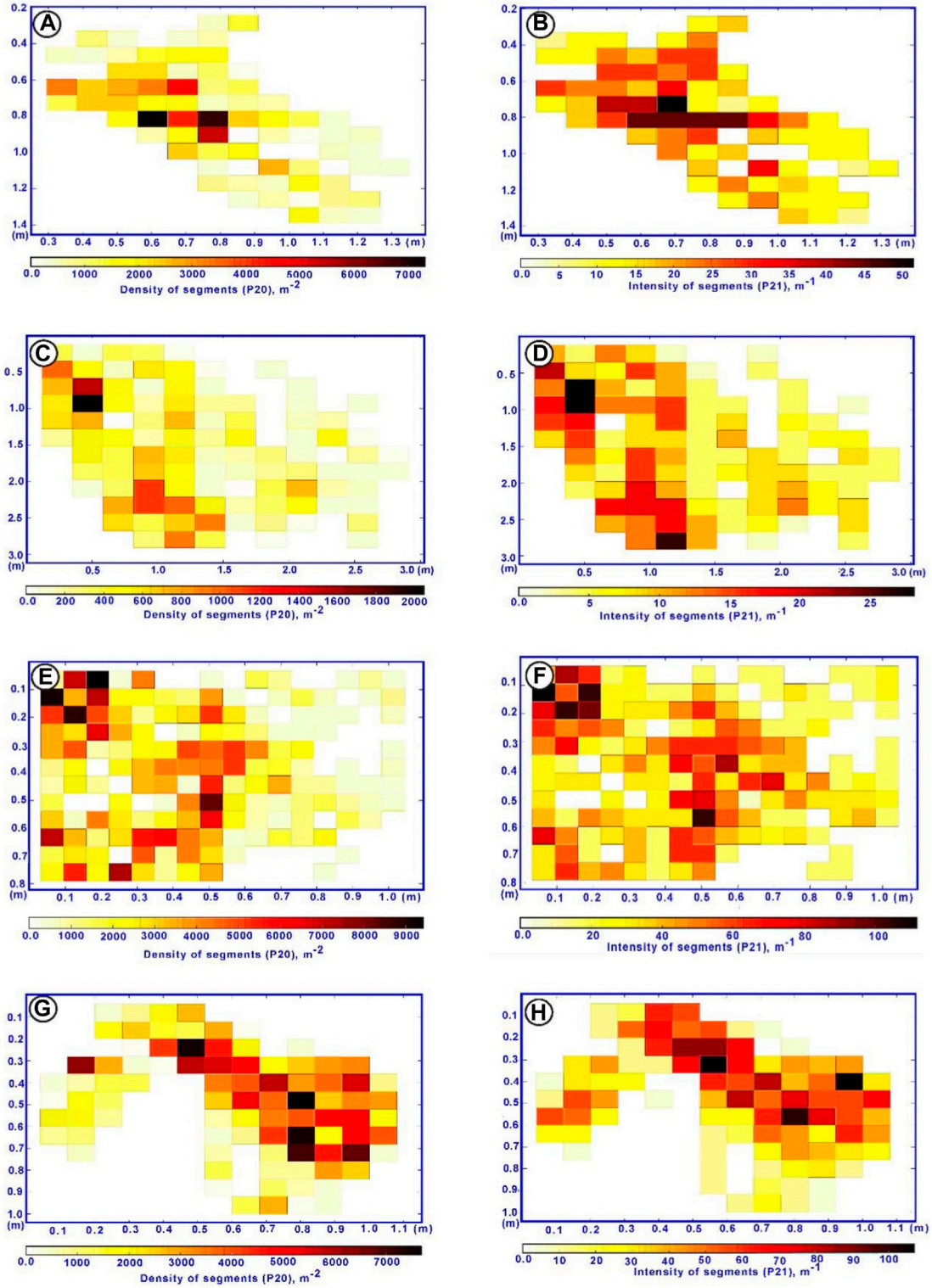

FIGURE 6
Estimated fracture density maps (P20) and estimated fracture intensity maps (P21). **(A,B)** P20 and P21 maps for fractured limestone in Wadi Nukhul; **(C,D)** P20 and P21 maps for fractured black limestone in Wadi Nukhul; **(E,F)** P20 and P21 maps for fractured basaltic dyke in Wadi Matulla; **(G,H)** P20 and P21 maps for fractured shale of Matulla Formation in Wadi Matulla.

(Figure 6B) revealed a high intensity (considerable fracture lengths per unit area) in two orientations, NW and NE. The second fracture network in Wadi Nukhul was carved on black limestone (Figure 6C), which revealed two or more distinct high-density clusters, with the highest-density clusters focused in the northwest and south. The black limestone's fracture intensity map (Figure 6D) exhibited high

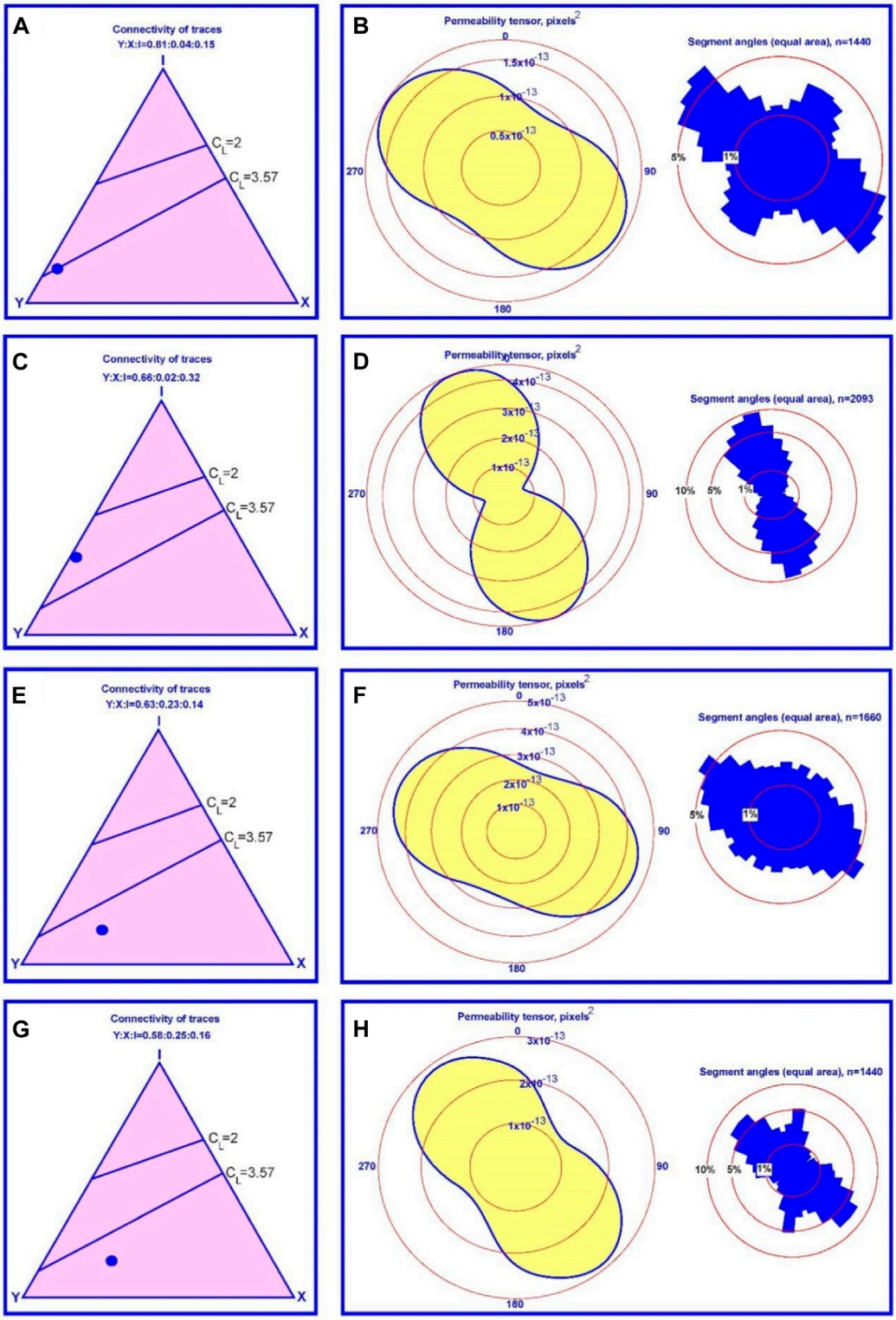

FIGURE 7
The estimated connectivity and 2D permeability ellipse of fracture networks for **(A–D)** Thebes limestone in Wadi Nukhul; **(E,F)** basaltic dike of Wadi Matulla; **(G,H)** shale in Wadi Matulla.

intensity in a zone extending from the south to the northwest. The density map of the fracture network on the Matulla dyke (Figure 6E) indicated three or more distinct high-density clusters, with the highest-density clusters in the NW. In addition, the fracture intensity map (Figure 6F) exhibited a high intensity in the NW and from south to north. The second fracture network was observed

on the shale in Wadi Nukhul (Figure 6G), which revealed three or more distinct high-density clusters. The fracture intensity map of shale (Figure 6H) displayed high intensity in a zone extending from the southeast to the northwest.

4.4 Fracture connectivity and permeability

In Wadi Nukhul, fracture connectivity and permeability estimation were the results of analyzing two different lithologies in FracPaQ. The connectivity plots (Figures 7A, C) were not similar, with the limestone fracture having a more significant proportion of "Y" and "X" nodes and a lower proportion of "I" nodes than black limestone, implying more excellent connectivity overall. Permeability estimation showed that the limestone fracture (Figure 7B) parallels the more extended, slightly higher-density fracture set than the other set-in azimuth of 130° (Figure 4C). For the black limestone, permeability (Figure 7D) was oriented parallel to the only longer, high-density fracture set in azimuth of 160°. In Wadi Matulla, the connectivity plots were similar, with the fracture of the basaltic dyke having a slightly higher proportion of "Y" nodes and a somewhat lower proportion of "X" nodes and "I" nodes than shale, reflecting more excellent connectivity overall (Figures 7E, G). Permeability estimation in Wadi Matulla showed that the fracture network of the basaltic dykes parallels the shorter, high-density fracture set in azimuth of 110° (Figure 7F). For the other location of the fractured shale, permeability was oriented parallel to the shorter, high-density fracture set in azimuth of 140° (Figure 7H).

4.5 Pore and fracture types

Based on the thin-section investigation of basalt dykes in Wadi Nukhul and Wadi Matulla, the pores were primary gas pores or vesicles, which are circular or sun-shaped closed pores filled with calcite (Figures 8A, B), and intergranular pores between crystals of calcite and quartz cements in fractures (Figure 8C, and Figures 9A, B). Many types of fractures originate from many mechanisms. The tectonic fractures result from tectonic events from the post-Miocene until the present. These fractures are encountered in sets paralleling or intersecting with high lengths and small or large widths (Figure 8D). The fractures originated from the cooling of basaltic magma were the shrinkage fractures that have different orientations and different widths with short lengths intersecting with each other and other fracture types (Figure 8E). The tectonic fractures intersect with others, forming an interconnecting network of fractures that facilitates the hydrocarbon flow that leads to high reservoir quality. Different fractures were partially or completely filled with calcite and quartz cements (Figure 8C; 9C,D). There was a late tectonic fracture in quartz cement, which was small in width and length and filled the large tectonic fractures (Figure 8F).

4.6 Petroleum systems models

4.6.1 Burial history model

The burial history models of wells ARS-6 and ARM-4 displayed the episodes of the pre-rift and syn-rift, which occurred in the Gulf of Suez, in addition to the basaltic intrusion event recorded in ARM-4 well between 24 and 22 Ma (Figure 10). The pre-rift episode characterized by low tectonic subsidence occurred from Early Cetaceous to Early Miocene (Aquitanian) represented by Nubia, Raha, Wata, Matulla, Duwi, Sudr, Esna, Mokattam, Thebes, Abu Zenima and Nukhul formations from base to top. The syn-rift episode was characterized by high tectonic subsidence that occurred through the Miocene from Burdigalian to Messinian, represented by Rudeis, Kareem, Belayim, South Gharib, and Ziet formations from older to younger. The OMBIs intruded into the pre-rift deposits as two distinct bodies. The lower OMBI was emplaced into the Matulla Formation with an apparent thickness of 132 m, and the upper OMBI was emplaced into the Sudr Formation with an apparent thickness of 90 m.

4.6.2 Thermal and maturation history models

In well ARS-6, the temperature distribution gradually increased with time and depth, reaching 170°C at a depth of 4200 m (Figure 10C). In well ARM-4, the temperature reached 180°C at depths ranging from 1000 m to 3500 m and from 24 (my) to recent due to the OMBI (Figure 10D).

In well ARS-6, the PRSRs of the Raha, Wata, and Duwi formations entered the early and mid-mature stages (Figure 10E). These source rocks entered the early mature stage in approximately 33 (my) at a depth of 1100 m, and the youngest PRSRs of the Esna and Thebes formations in 14 (my). The PRSRs Raha, Wata, and Duwi formations met the mid-mature stage in 12 (my) at a depth of 1800 m, whereas the youngest PRSRs began the mid-mature stage in 2 (my) at 2800 m of the Esna and Thebes formations. In well ARM-4, the PRSRs of the Nubia, Raha, Wata, and Duwi formations began the early mature stage in 23.5 (my) at a depth of 1000 m, while the PRSRs of Esna and Sudr began this stage in 22.9 my at a depth of 440 m (Figure 10F). The Nubia, Raha, Wata, and Duwi formations met the mid-mature stage in 22.9 my at a depth of 1000 m, whereas Esna and Sudr met this stage in 22.5 my at a depth of 600 m. The late mature stage has been met by the oldest PRSRs in 22.3 my at a depth of 1000 m, while the youngest PRSRs met this stage in 2.2 my at a depth of 3200 m. Mid- and late-mature stages continue till the present, while the early-mature stage ended in 4.5 my.

4.6.3 Hydrocarbon generation model

In well ARS-6, the early generation phase for the PRSRs of Raha, Wata, and Duwi formations onset in 13 my at 1800 m, whereas the PRSRs of Esna and Thebes formations onset this stage in 4 my at 3100 m (Figure 11A). The main phase generation for the PRSRs of Raha, Wata and Duwi formations began in 8.0 my at 2100 m, while for the Esna and Thebes formations, it began in 3.3 my at 3150 m. The peak-late generation for the Raha, Wata, and Duwi began in 3.1 my at 3400 m, whereas the Esna and Thebes formations began this stage in 1.6 my at 3120 m. This stage ended in 1.3 my for the lower boundary for the PRSRs of Raha and Wata formations, while this stage continues till present for the upper boundary and the PRSR Duwi Formation. Moreover, for the PRSRs Thebes and Esna formations, the main phase generation continues till the present. In well ARM-4, the PRSRs of Raha,

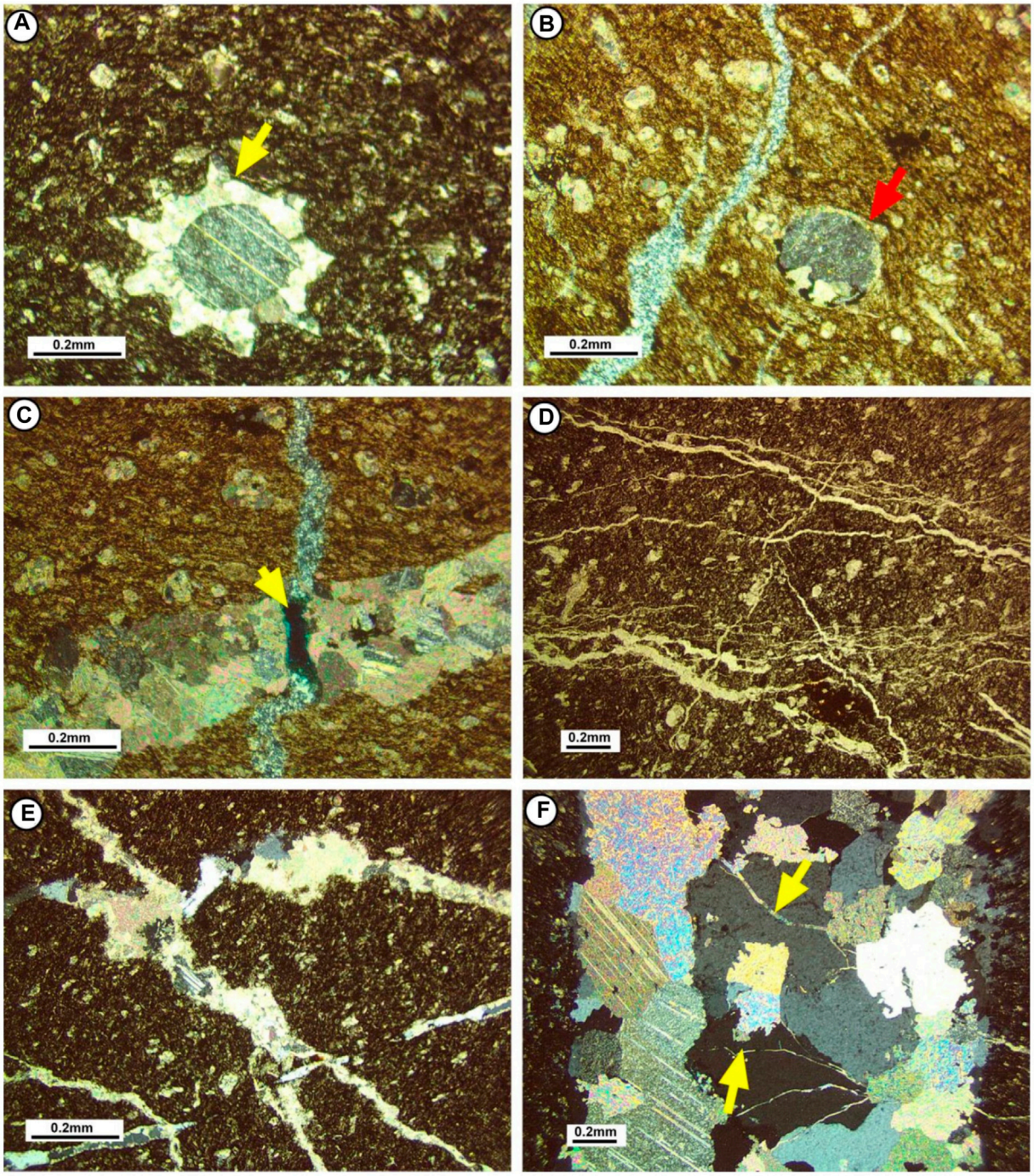

FIGURE 8
Thin-section photomicrographs of basaltic dyke in Wadi Matulla showing **(A)** closed sun-like gas pore filled with calcite; **(B)** closed circular gas pore filled with calcite; **(C)** intercrystalline pore between fracture filled with calcite and intersected with fracture filled with quartz; **(D)** tectonic fractures; **(E)** shrinkage fractures; **(F)** late tectonic fractures in quartz cement.

Wata, and Duwi formations began the early main and peak-late generation phases in 23.9, 23.6, and 22.9 my and ended in 23.6, 22.9, and 22.1 my, respectively, at a depth of 1000 m (Figure Figure11B). The PRSR Sudr Formation began the three-generation phases as the same in the Raha and Wata formations, while the peak-late phase continues till the present at a depth of 3000 m. The PRSR of Esna Formation met the early, main, and peak-late generation phases in 22.7, 4.1, and 3.6 (my) at depths of 450 m, 2860 m, and 3000 m, respectively, and the peak-late generation phase ended in 1.0 my.

4.6.4 Transformation ratio

In well ARS-6, the PRSR of Thebes Formation passed the early and main generation phases with a maximum transformation ratio

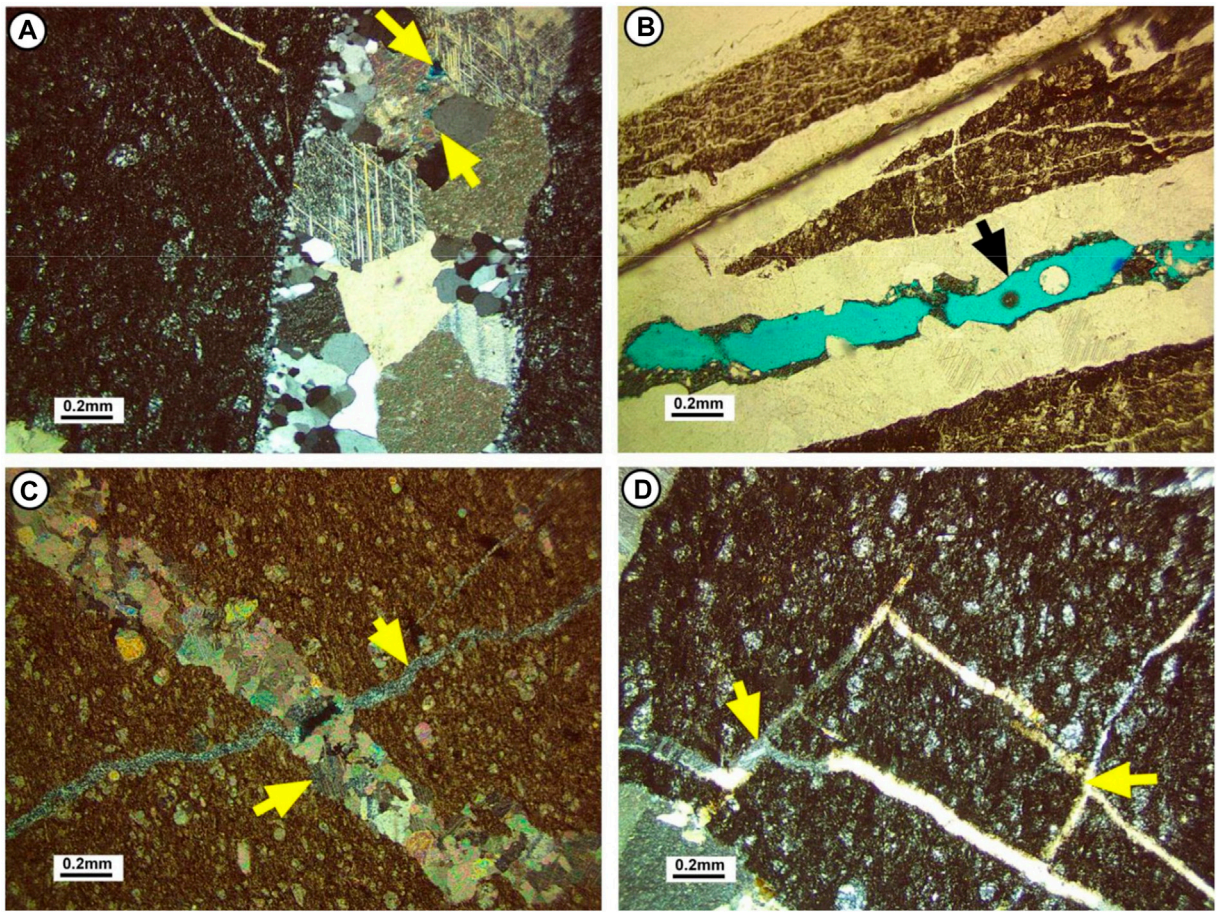

FIGURE 9
Thin-section photomicrographs showing **(A)** intercrystalline pores in Wadi Nukhul basaltic intrusion; **(B)** intercrystalline pores in Wadi Matulla basaltic intrusion; **(C,D)** interconnected fractures showing good fracture networks in Wadi Nukhul basaltic intrusion. .

of 56% (Figure 11C). The PRSR of Esna Formation met the main and peak-late generation phases with a maximum transformation ratio of 64%. The PRSR of the Duwi Formation passed the peak-late generation phase with a maximum transformation ratio of 80%. The PRSRs of the Wata and Raha formations passed the peak-late generation phase with maximum transformation ratios of 85% and 100%, respectively. In well ARM-4, the PRSRs Esna, Sudr, and Duwi formations met the peak-late generation phase with maximum transformation ratios of 95%, 95%, and 100%, respectively, while the PRSRs Wata and Raha formations passed the peak-late generation phase with transformation ratios of 100% (Figure 11D).

4.6.5 Expulsion history model

In well ARS-6, the expelled oil from the PRSRs of Esna and Duwi formations was 1.9 and 2.6 kg/m^3, respectively, whereas the expelled oil for the PRSRs of Wata, Raha, and Nubia formations was 3.2 3.7 and 3.8 kg/m^3, respectively (Figure 11E). In well ARM-4, the expelled oil from PRSRs Esna, Sudr, and Duwi formations was 3.3, 2.2, and 18 kg/m^3, respectively (Figure 11F). The maximum expelled oil from PRSRs Wata, Raha, and Nubia formations was 5.0, 5.1, and 5.8 kg/m^3, respectively.

5 Discussion

5.1 The impact of OMBI on temperature and mature stages

The effect of OMBI was investigated through the correlation of the maturity, generation, transformation ratio, and expulsion between well ARM-4 with OMBI and well ARS-6 without OMBI recorded. In well ARS-6, the highest temperature is 170°C at 4100 m, while in well ARM-4, the highest temperature is 180°C first recorded at a depth of 1000 m attributed to the OMBI intrusion (Figures 11A, B). Moreover, at the maximum drilled depth of 3500 m, the temperature is 180°C. At the same depths in both wells, the temperature differs; for example, at a depth of 1000 m, the temperature reached 75°C in well ARS-6, while in well ARM-4, it reached 180°C. The pronounced difference in temperature distribution between both wells was due to the occurrence of OMBI in well ARM-4.

The high temperature distribution in well ARM-4 positively affects the PRSRs maturity, particularly at shallow depths. The early mature stage began at a depth of 1000 m in well ARS-6, while it began at 450 m in well ARM-4 (Figures 12A, B). Furthermore, in wells ARS-6 and ARM-4, the mid-mature stage occurred at depths of

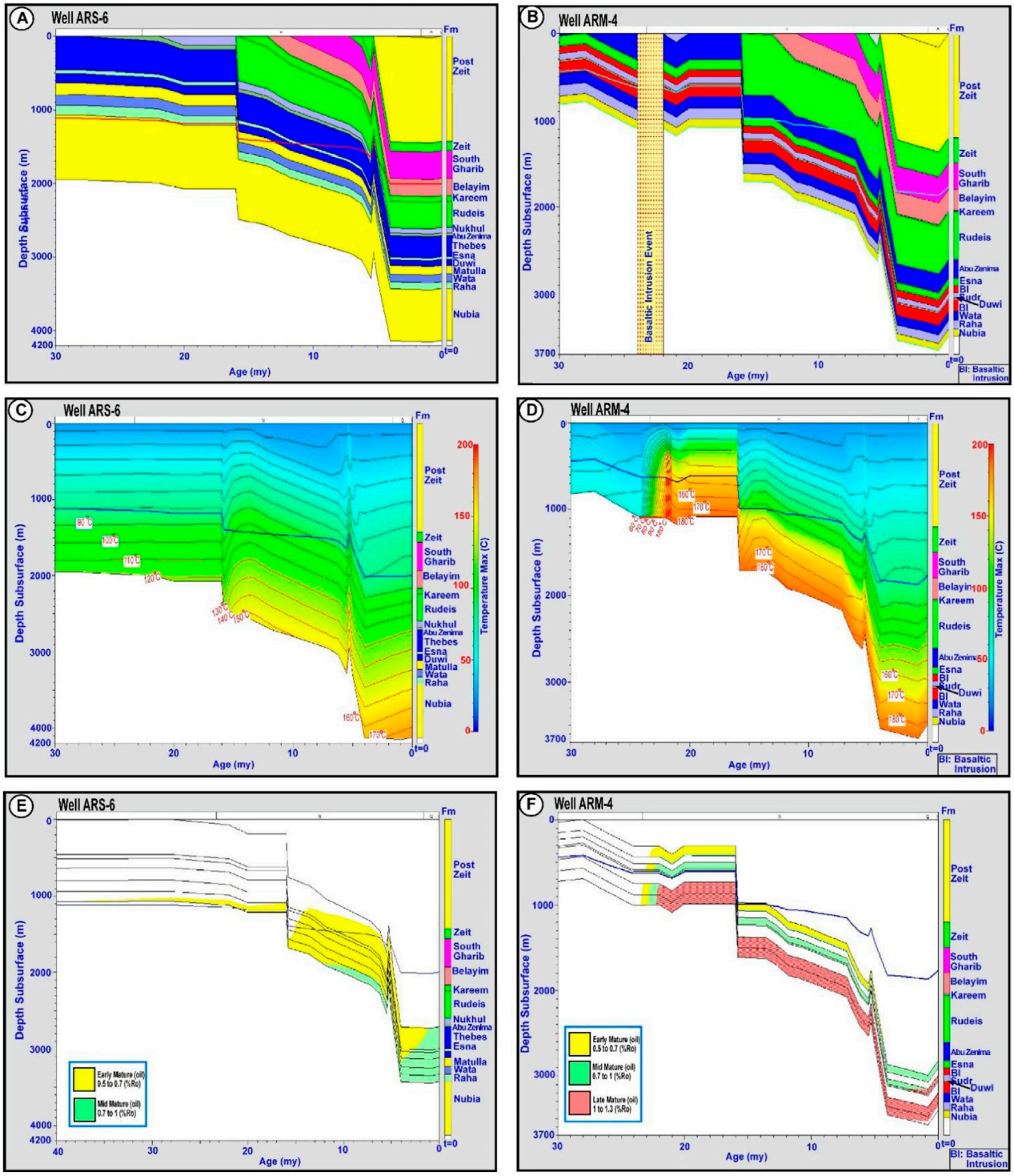

FIGURE 10
(A) Burial history model for well ARS-6; **(B)** burial history model for well ARM-4 showing the basaltic intrusion event occurred between 24 and 22 my; **(C)** temperature distribution model for well ARS-6; **(D)** temperature distribution model for well ARM-4; **(E)** mature stages model for well ARS-6; **(F)** mature stages model for well ARM-4.

1900 m and 600 m, respectively. Additionally, in well ARS-6, the PRSRs only met early and mid-mature stages, whereas, in well ARM-4, they met early, mid-, and peak-late mature stages for long durations. In well ARM-4, PRSRs attained high maturity at shallow depths. In well ARS-6, the early generation phase of the oldest PRSRs began in 13 my at a depth of 1800 m, whereas in well

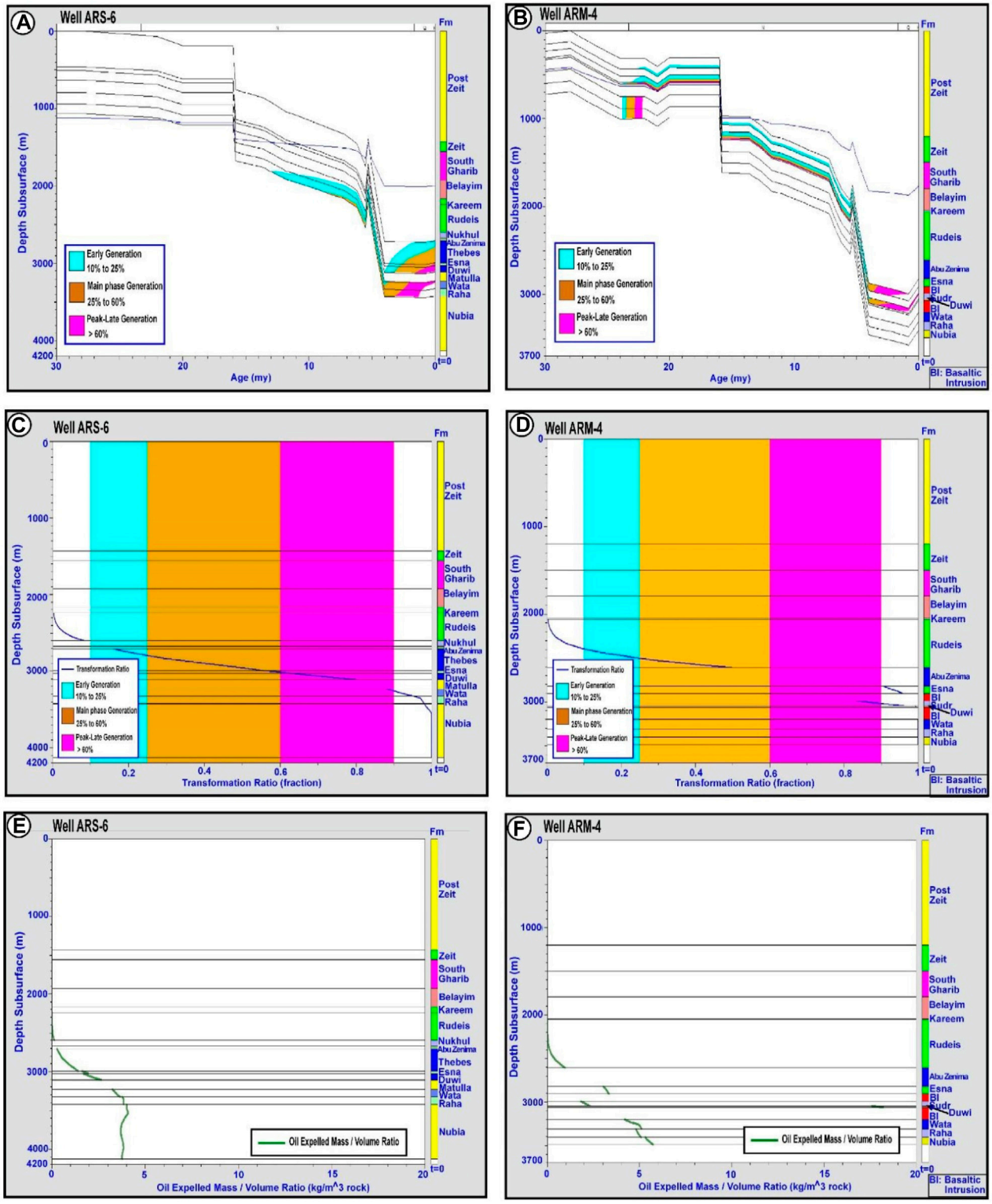

FIGURE 11
(A) Hydrocarbon generation phases model for well ARS-6; **(B)** generation phases model for well ARM-4; **(C)** transformation ratio model for well ARS-6; **(D)** transformation ratio model for well ARM-4; **(E)** oil expulsion model for well ARS-6; **(F)** oil expulsion model for well ARM-4.

ARM-4, this stage began in 24 (my) at a depth of 1000 m. In well ARS-6, the main generation phase began in 8.5 (my) at 2100 m, and in well ARM-4, it began in 23.6 (my) at depths of 1000 m and 600 m for the oldest and youngest PRSRs, respectively. In well ARS-6, the peak-late generation phase began in 3.3 my at 3400 m, whereas in well ARM-4, it occurred in 22.8 my and 3.1 my at depths of 1000 m

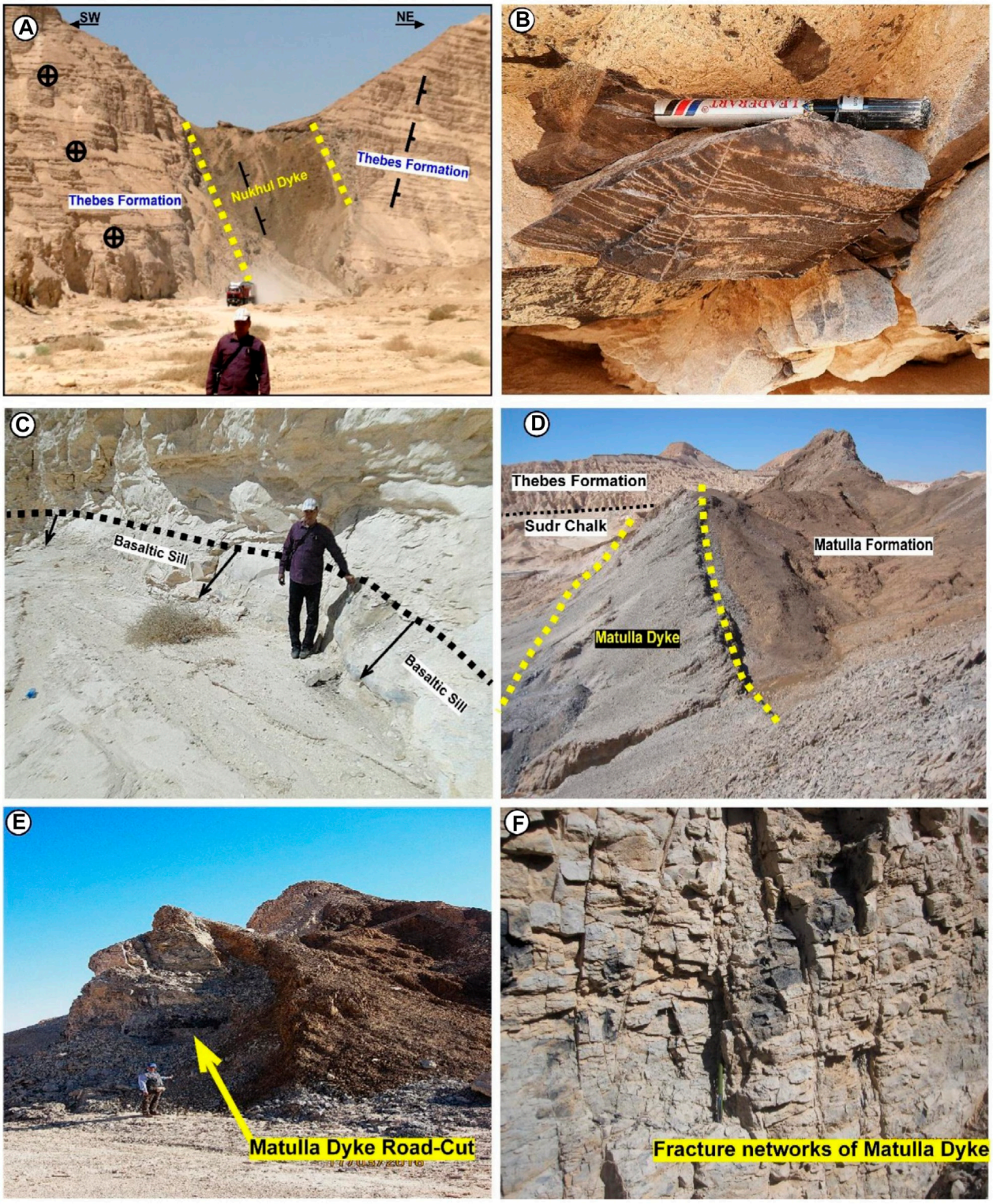

FIGURE 12
Field photos showing **(A)** Wadi Nukhul basaltic dyke intruded in Thebes Formation; **(B)** fractures parallel to the bedding in black limestone near the contact with the dyke; **(C)** basaltic sill branching out from Nukhul dyke with its upper boundary only exposed; **(D)** Wadi Matulla basaltic dyke intruded in Matulla Formation; **(E)** road cut of the basaltic Matulla dyke; **(F)** fracture networks of the Matulla dyke.

and 3100 m for oldest and youngest PRSRs, respectively. High maturity stages and generation phases are reflected by transformation ratio and expelled oil; for example, the Duwi Formation attained the highest transformation ratio of 100% and expelled oil of 18.3 kg/m^3 in well ARM-4, while they reached 80% and 2.6 kg/m^3 in well ARS-6 (Supplementary Table S2).

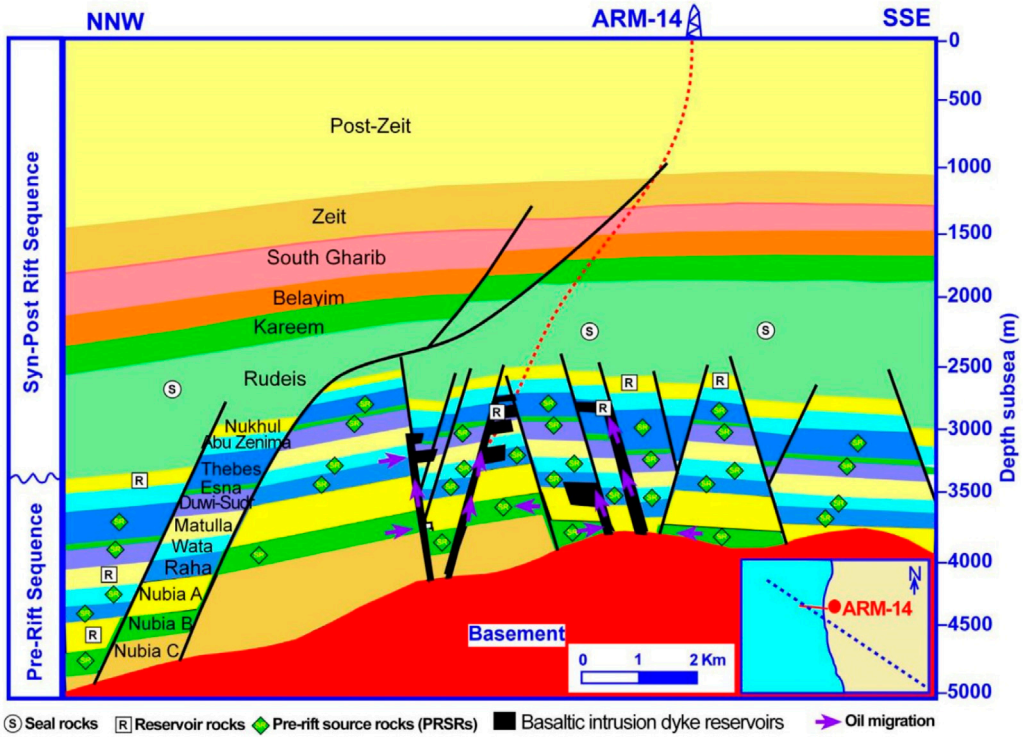

FIGURE 13
Geological cross-section through the Abu Rudeis-Sidri Field showing basaltic intrusion reservoirs distribution and the petroleum system elements source rocks, reservoir rocks, and seal rocks, in addition to the direction of oil migration (Modified after Abd El-Gawad et al., 2022).

5.2 Timing of basaltic intrusion, source rock maturity, and hydrocarbon generation

The thermal impact of sill intrusion increases vitrinite reflectance, a maturity indicator, in zones below and above the sill (Zhu et al., 2007). The effect decreases with distance from the contact The basaltic intrusion occurred between 24 and 22 my, and the youngest Thebes Formation deposited in 50.6 my. This implies that the basaltic intrusion intruded in all the PRSRs and consequently has a high thermal impact on these source rocks. The thermal impact is reflected in the acceleration of the maturity and generation of in well ARM-4 compared to well ARS-6.

In well ARM-4, the Nubia began the maturity as an early mature stage in 23.74 my, the Sudr Formation reached this stage in 2.17 my, and the Esna Formation did not reach this stage (Supplementary Table S3). The maturity duration extended from the onset of OMBI in 24 my to 0.05 my. In well ARS-6, the maturity began earlier in 50 my and all the PRSR did not reach the late mature stage except the Nubia Formation, whose bottom only entered the late stage in 13.45 my. In well ARM-4, all the PRSRs passed the late mature stages except the Esna Formation, while in well ARS-6, the PRSRs did not pass this stage except the bottom of the Nubia Formation.

In well ARM-4, the generation of PRSRs began as an early phase in 23.80 my and reached the peak-late phase that ended in 3.1 my (Supplementary Table S4). In well ARS-6, the generation commenced in 48.16 my, during which all formations except the tops of Thebes and Esna formations reached the main phase. Additionally, the top of the Duwi Formation did not reach the peak-late phase.

5.3 Thermal impact and distribution style of OMBI

The thermal maturity of the dyke intrusion is proportional to its thickness (Bishop and Abbott, 1995). The thickness of dykes in the Abu Zenima and Hammam Faraoun areas ranges from 10 to 30 m (Ragab and El-Kaliouby, 1992). In the Wadi Matulla area, a very high geothermal gradient accompanied by a rift-related Oligocene basaltic dyke resulted in the carbonization of the kerogen-bearing Upper Cretaceous Sudr Chalk over a 100 m wide baked zone. At the time of intrusion, the maximum temperature on the Matulla dyke contact was 500°C and decreased to 100°C far away from the contact (Sharib et al., 2019).

The thickness of Wadi Nukhul and Wadi Matulla dykes is approximately 30 m. Wadi Nukhul dyke intruded in PRSR Thebes Formation, resulting in the dipping of its eastern side to the northeast direction with an angle of about 10□. In contrast, on the western side, the Thebes Formation is horizontal (Figure 12A). On contact with the dyke, the Thebes limestone was thermally altered to black, dark gray, and gray limestones, and the thermal alteration disappeared within about 15 m from the dyke contact. Within 5 m from the contact with the dyke, Thebes limestone source rock was highly mature with fractures parallel to the bedding (Figure 12B). These fractures of Thebes source rock indicated high oil expulsion due to high maturity and the generation that facilitated the oil flow from Thebes source rock to the basaltic dyke reservoir. On the western side of the Nukhul dyke and near the contact appears the basaltic sill branched out from the main dyke

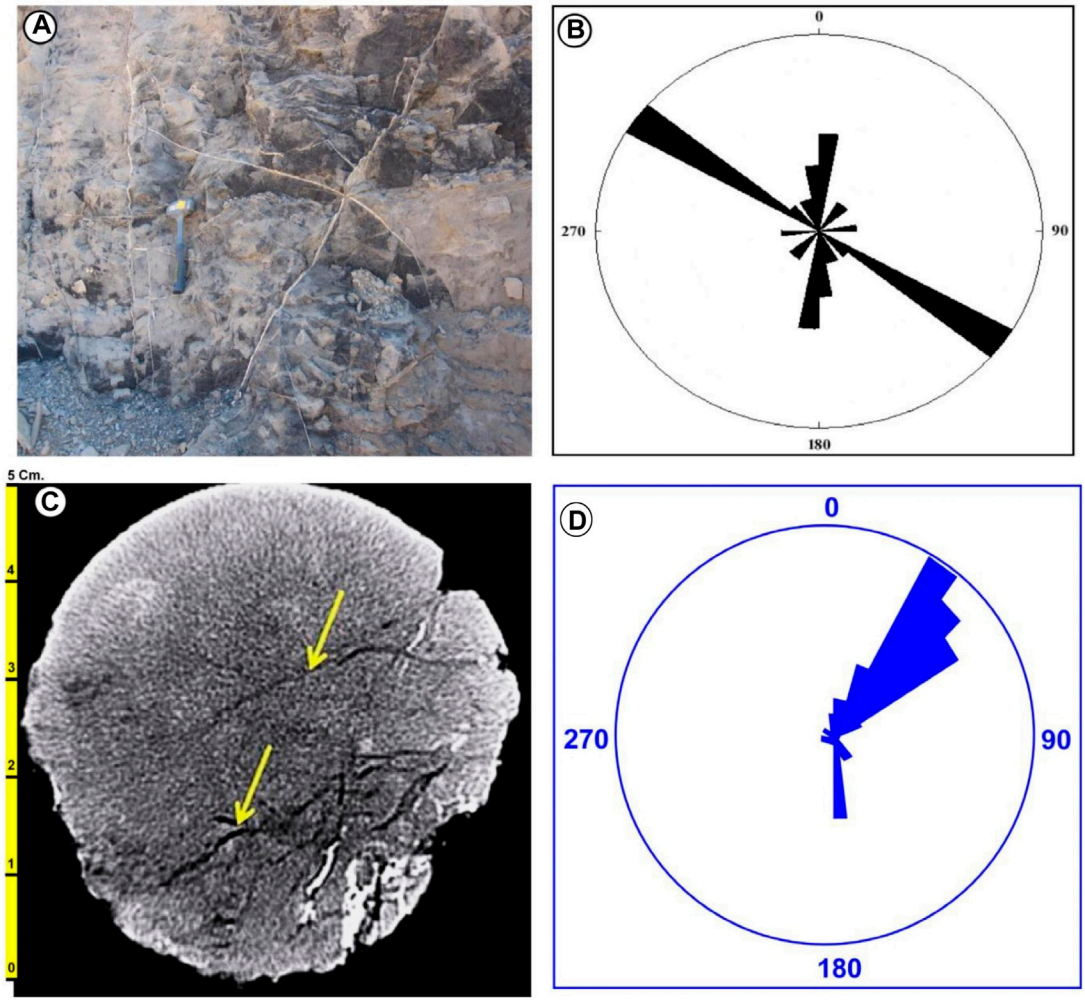

FIGURE 14
Field photos showing **(A)** fracture network in Matulla basaltic dyke; **(B)** Matulla dyke; **(C)** core photo of OMBI reservoir in Abu Rudeis-Sidri field showing the fractures network; **(D)** a rose diagram showing the fracture orientations for OMBI reservoir (**C,D** combined from Abd El-Gawad et al., 2022).

and parallel to the bedding plain with a thickness of 1m above the ground (Figure 12C). This distribution style of vertical dyke with horizontal sill increases the thermal maturity as it extends horizontally as sills, increases the exposed area of the source rock to thermal alteration and high thermal maturity. Wadi Matulla dyke intruded in PRSR of Duwi, Sudr Chalk, and Matulla formations with dip angle nearly vertical (Figure 12D). At the begging of the Wadi Matulla, Matulla basaltic dyke occurred as a road cut that aids in studying the fracture pattern as an analog of the basaltic reservoir in Abu Rudeis-Sidri field (Figures 12E, F).

The main oil production in the Abu Rudeis-Sidri field comes from the pre-rift reservoirs of the Nubia A, Matulla, and Nukhul formations. A geological cross-section has been created based on the interpretation of a seismic section through the field to illustrate the subsurface distribution of OMBI (Figure 13). The basaltic intrusions in this area are vertical dykes with perpendicular sills that intrude horizontally and parallel to the bedding. These dykes have penetrated the pre-rift formations, including source rocks such as Nubia B, Raha, Wata, Duwi, Sudr, and Thebes formations, as well as reservoirs like Nubia A, Matulla, and Nukhul formations. In the ARM-4 well, there are two zones of basaltic intrusions: a lower zone that intruded into the PRSR Duwi Formation with a thickness of 136 m and an upper zone that intruded into the Esna and Sudr formations with a thickness of 81 m (S. Table 1). It is important to note that the high thickness of basaltic intrusions in the ARM-4 well is not their true thickness but rather their apparent thickness due to the drilling path penetrating vertically within the basaltic intrusions as a dyke. The thicknesses of these intrusions include metasediments resulting from the thermal effect of basaltic intrusions. The distribution style of dykes with sills can be observed in well ARM-14 on the geological cross-section based on interpreted seismic data.

5.4 Reservoir quality of OMBI

The development of high-quality volcanic reservoirs is primarily influenced by lithology and lithofacies, weathering and corrosion, as well as fractures (Yiming et al., 2023). The fracture network distribution in the surface analog Matulla dyke and subsurface Abu Rudeis-Sidri basaltic intrusions is responsible for the reservoir

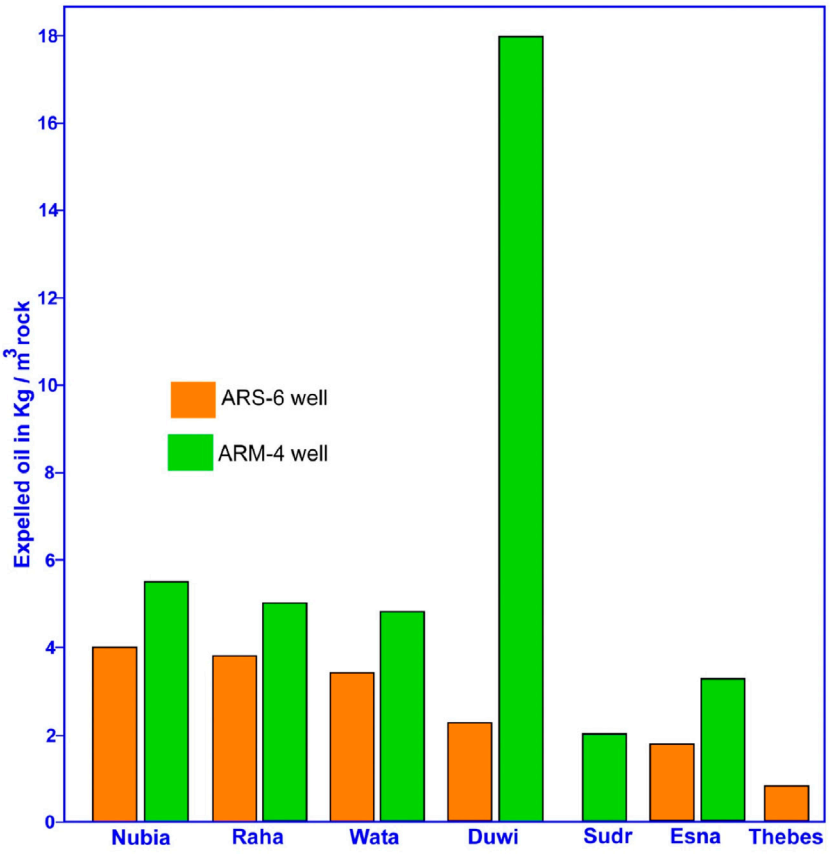

FIGURE 15
Histogram showing the expelled oil from the pre-rift source rocks for wells ARS-6 and ARM-4 in Abu Rudeis field.

quality of these intrusions. In the Matulla basaltic dyke, fractures range in length from a few centimeters to 2 m, with widths ranging from a few millimeters to a few centimeters. These fractures are visible as intersected white lines filled with calcite (Figure 14A). The main structural trends of these fractures in the Gulf of Suez are northwest-southeast and northeast-southwest (Figure 14B). Similarly, the subsurface basaltic intrusions in the Abu Rudeis-Sidri field also exhibit fractures with a main trend of the northeast-southwest direction (Figures 14C, D).

Lee et al. (2021) evaluated the alteration degree by integrating petrophysical properties with mineralogical and geochemical analysis. They classified the alteration into four stages from fresh to slightly altered, weakly altered, moderately altered, and strongly altered. The identified alteration phases have affected the reservoir quality of the basaltic intrusions in the study area. Reservoir properties were primarily influenced by lithology, as well as mineralogical and textural variations. The fracture networks observed in the Matulla basaltic dyke show high connectivity and permeability. Thin sections of the basaltic dykes reveal that porosity originates from primary pore types such as gas and vesicles, as well as shrinkage and tectonic fractures that are interconnected, creating fracture networks with high porosity and permeability. Hydrothermal alteration was intense in permeable zones of fractured and weathered basaltic dykes, facilitating fluid circulation (Navelot et al., 2018; Caspari et al., 2020). The hydrocarbon potential is influenced by the distribution style of basaltic intrusions in three ways. Firstly, the intrusion of basaltic dykes into the PRSRs allows for oil collection through rock fracturing from these mature rocks. Secondly, sills branching out from the dykes increase the thermal effect of the basaltic intrusions. Lastly, fracture networks in the host rocks ensure efficient oil expulsion from these rocks to the basaltic intrusions and facilitate its flow from mature source rocks to the basaltic intrusion reservoir.

5.5 Impact of OMBI on the petroleum system in the Abu Rudeis-Sidri Field

The impact of basaltic intrusions on thermal maturity is demonstrated by comparing the transformation ratio and expelled oil in the ARS-6 well without basaltic intrusions and the ARM-4 well with basaltic intrusions (Figure 15). However, the PRSR Nubia has equal transformation ratios in both wells and exhibits different amounts of expelled oil. In the ARS-6 well, the Nubia source rock expels 4 kg/m^3 of oil, whereas in the ARM-4 well, it reaches 5.5 kg/m^3. Similarly, in the ARS-6 well, PRSRs Raha Wata and Duwi expel 3.8, 3.4, and 2.25 kg/m^3 of oil, respectively, whereas in the ARM-4 well, they expel 5, 4.8, and 18 kg/m^3, respectively. The Esna source rock expels 1.75 and 3.15 kg/m^3 of oil in the ARS-6 and ARM-4 wells, respectively. The amount of expelled oil from PRSRs in the ARM-4 well increases twofold compared to that from the

same source rocks in the well ARS-6 due to the high thermal maturity experienced by basaltic intrusions.

The Matulla and Nukhul dykes, which serve as surface analogs for the basaltic intrusion reservoir, are highly fractured and have well-connected networks, resulting in high levels of porosity and permeability. In 2014, exploring these basaltic intrusions as oil producer reservoirs in the Abu Rudeis-Sidri field led to a doubling of oil production (Abd El-Gawad et al., 2021; 2022). The basaltic intrusion reservoir collects an equivalent amount of oil to all the pre-rift reservoirs in the Nubia, Matulla, and Nukhul formations. This is supported by production data showing a doubling of production rates after tapping into the basaltic intrusion reservoir. The distribution pattern of the basaltic intrusion dykes greatly influences the collection of oils from the pre-rift petroleum system. These dykes vertically penetrate all the PRSRs, allowing expelled oil to flow directly from these mature source rocks into the highly fractured basaltic intrusion reservoirs.

The intrusion of igneous sills and dykes into prospective sedimentary basins can have significant impacts on petroleum systems (Holford et al., 2013). Several factors influence the pre-rift petroleum system in the Abu Rudeis-Sidri field, including how basaltic intrusions enhance the thermal maturity of PRSRs, oil generation, transformation ratio, and amount of expelled oil. The high-quality basaltic intrusion reservoir is attributed to interconnected fractures of various types developed throughout the tectonic history of the Gulf of Suez rift basin. Additionally, shale deposits from the Rudeis Formation with high thickness act as seals for pre-rift reservoirs, preserving migrated oil within these reservoirs.

6 Conclusion

This study investigated the effects of basaltic intrusions on source rock maturity and hydrocarbon potential in the Abu Rudeis-Sidri oil field, Gulf of Suez, Egypt. Field studies of two basaltic dykes showed they have high fracture density, intensity, connectivity, and permeability. Thin sections revealed primary pores and interconnected fractures, indicating good reservoir quality. Subsurface studies compared two wells - one with basaltic intrusions (ARM-4) and one without (ARS-6). The intrusions in ARM-4 led to higher temperatures and maturity at shallower depths *versus* ARS-6. ARM-4 source rocks reached all maturity stages and generation phases, had a higher transformation ratio, and expelled more oil. Basaltic intrusions, as dykes with branching sills, significantly impacted source rock thermal maturity. They increased oil expulsion into the highly fractured basaltic reservoirs. Production from these unconventional reservoirs was equivalent to all conventional reservoirs. This study demonstrates basaltic intrusions' effects on petroleum systems and their potential as unconventional reservoirs. The fracture patterns identified in outcrops can help locate similar unexplored reservoirs in the Gulf of Suez.

Data availability statement

The raw data supporting the conclusion of this article will be made available by the authors, without undue reservation.

Author contributions

KE: Validation, Writing–original draft, Writing–review and editing, Conceptualization, Data curation, Investigation, Methodology, Supervision, Visualization. MB: Investigation, Methodology, Validation, Writing–original draft, Writing–review and editing, Resources. MG: Methodology, Resources, Writing–original draft, Writing–review and editing, Data curation, Formal Analysis. PS: Conceptualization, Investigation, Supervision, Validation, Writing–review and editing. ME: Data curation, Resources, Writing–original draft, Writing–review and editing, Software, Validation, Visualization. MA: Resources, Validation, Writing–original draft, Writing–review and editing, Project administration. AE-S: Formal Analysis, Funding acquisition, Investigation, Methodology, Project administration, Resources, Writing–original draft, Writing–review and editing. AA: Conceptualization, Investigation, Methodology, Validation, Visualization, Writing–original draft, Writing–review and editing.

Funding

The author(s) declare financial support was received for the research, authorship, and/or publication of this article. The authors extend their appreciation to the Deputyship for Research and Innovation, "Ministry of Education" in Saudi Arabia for funding this research (IFKSUOR3—296—1).

Acknowledgments

The authors express their gratitude to the Egyptian General Petroleum Corporation (EGPC) and Petrobel Petroleum for generously providing the necessary subsurface data to carry out a part of this study. The authors extend their appreciation to the Deputyship for Research and Innovation, "Ministry of Education" in Saudi Arabia for funding this research (IFKSUOR3—296—1).

Conflict of interest

The authors declare that the research was conducted in the absence of any commercial or financial relationships that could be construed as a potential conflict of interest.

Publisher's note

Supplementary material

The Supplementary Material for this article can be found online at: https://www.frontiersin.org/articles/10.3389/feart.2023.1295271/full#supplementary-material

References

Aarnes, I., Planke, S., Trulsvik, M., and Svensen, H. (2015). Contact metamorphism and thermogenic gas generation in the Vøring and Møre basins, offshore Norway, during the Paleocene–Eocene thermal maximum. *J. Geol. Soc. Lond.* 172, 588–598. doi:10.1144/jgs2014-098

Aarnes, I., Svensen, H., Connolly, J. A. D., and Podladchikov, Y. Y. (2010). How contact metamorphism can trigger global climate changes: modeling gas generation around igneous sills in sedimentary basins. *Geochim. Cosmochim. Acta* 74, 7179–7195. doi:10.1016/j.gca.2010.09.011

Aarnes, I., Svensen, H., Polteau, S., and Planke, S. (2011). Contact metamorphic devolatilization of shales in the Karoo Basin, South Africa, and the effects of multiple sill intrusions. *Chem. Geol.* 281, 181–194. doi:10.1016/j.chemgeo.2010.12.007

Abdel Aal, A. Y. (1998). Mineral and chemical composition of basalts in the neighbourhood of Giza, Egypt. *J. Afr. Earth Sci.* 26, 101–117. doi:10.1016/s0899-5362(97)00139-5

Abd El-Gawad, E., Fathy, M., Mosad, M., Refaat, A., and Metwally, A. (2022). Fracture recognition and characterization of the unconventional igneous intrusion reservoir in rudeis-sidri field, gulf of suez, Egypt. *J. Geol. Geophys. 1 J. Geol. Geophys* 11, 1001012. doi:10.35248/2381-8719-22.11.1012

Abd El-Gawad, E. A., Mohamed, M. F., Mohamed, M. M., Alian, A. H., Metwaly, A. M., and Ameen, S. S. (2021). Geology delineating the geometry and modeling of the unconventional igneous intrusions by seismic attributes; a case study in Rudeis-Sidri Field, Gulf of Suez, Egypt. *DJS* 43, 80–88. doi:10.21608/DJS.2021.187497

Abuseda, H., Kassab, M. A., LaLa, A. M., and El Sayed, N. A. (2015). Integrated petrographical and petrophysical studies of some Eocene carbonate rocks, Southwest Sinai, Egypt. *Egypt. J. Pet.* 24, 213–230. doi:10.1016/j.ejpe.2015.05.006

Abu Shama, A., El-Nahrawy, S., and Farouk, S. (2023). Age assignment, palaeoecology and sequence stratigraphic framework of the Nukhul formation at wadi baba, west-central sinai (Egypt). *Palaeobiodiversity Palaeoenvironments* 103, 775–798. doi:10.1007/s12549-023-00580-4

Alsharhan, A. S. (2003). Petroleum geology and potential hydrocarbon plays in the Gulf of Suez rift basin, Egypt. *Am. Assoc. Pet. Geol. Bull.* 87, 143–180. doi:10.1306/062002870143

Alsharhan, A. S., and Salah, M. G. (1994). Geology and hydrocarbon habitat in a rift setting: southern Gulf of Suez, Egypt. *Bull. Can. Pet. Geol.* 42, 312–331. doi:10.35767/gscpgbull.42.3.312

Alsharhan, A. S., and Salah, M. G. (1997). Lithostratigraphy, sedimentology and hydrocarbon habitat of the pre-cenomanian nubian sandstone in the gulf of suez oil province, Egypt. *GeoArabia* 2, 385–400. doi:10.2113/geoarabia0204385

Ayyad, H. M., Hewaidy, A. G. A., Farouk, S., Samir, A., and Bazeen, Y. S. (2023). Sequence stratigraphy of the upper Oligocene–middle Miocene succession in west–central Sinai, Egypt. *Geol. J.* 58, 264–282. doi:10.1002/gj.4590

Badawy, A., and Abdel-Fattah, A. K. (2006). 2001 august earthquake swarm at shadwan island, gulf of suez, Egypt. *Geophys. J. Int.* 167, 288–296. doi:10.1111/j.1365-246x.2006.03094.x

Baldridge, W. S., Eyal, Y., Bartov, Y., Steinitz, G., and Eyal, M. (1991). Miocene magmatism of sinai related to the opening of the Red Sea. *Tectonophysics* 197, 181–201. doi:10.1016/0040-1951(91)90040-y

Barakat, H. (1982). "Geochemical criteria for source rock, Gulf of Suez," in *Proceedings* (Egypt: Sixth EGPC Exploration Seminar), 224–251.

Beleity, A. (1982). "The composite standard and definition of paleo events in the Gulf of Suez," in *6th EGPC* (Cairo: Explor. Seminar).

Bishop, A. N., and Abbott, G. D. (1995). Vitrinite reflectance and molecular geochemistry of Jurassic sediments: the influence of heating by Tertiary dykes (northwest Scotland). *Org. Geochem.* 22, 165–177. doi:10.1016/0146-6380(95)90015-2

Bosworth, W., Huchon, P., and McClay, K. (2005). The red sea and gulf of aden basins. *J. Afr. Earth Sci.* 43, 334–378. doi:10.1016/j.jafrearsci.2005.07.020

Bosworth, W., and McClay, K. (2001). Structural and stratigraphic evolution of the Gulf of Suez rift, Egypt: a synthesis. *Mémoires Du. Muséum Natl. d'histoire Nat.* 186, 567–606.

Bosworth, W., and Stockli, D. F. (2016). Early magmatism in the greater Red Sea rift: timing and significance. *Can. J. Earth Sci.* 53, 1158–1176. doi:10.1139/cjes-2016-0019

Brekke, T., Krajewski, K. P., and Hubred, J. H. (2014). Organic geochemistry and petrography of thermally altered sections of the middle triassic botneheia formation on south-western edgeøya, svalbard. *Nor. Pet. Dir. Bull.* 11, 111–128.

Caspari, E., Greenwood, A., Baron, L., Egli, D., Toschini, E., Hu, K., et al. (2020). Characteristics of a fracture network surrounding a hydrothermally altered shear zone from geophysical borehole logs. *Solid earth* 11, 829–854. doi:10.5194/se-11-829-2020

Chen, Z., Wang, X., Zha, M., Zhang, Y., Cao, Y., Yang, D., et al. (2016). Characteristics and formation mechanisms of large volcanic rock oil reservoirs: a case study of the Carboniferous rocks in the Kebai fault zone of Junggar Basin, China. *Am. Assoc. Pet. Geol. Bull.* 100, 1585–1617. doi:10.1306/04151614066

Chen, Z., Yan, H., Li, J., Zhang, G., Zhang, Z., and Liu, B. (1999). Relationship between tertiary volcanic rocks and hydrocarbons in the liaohe basin, people's Republic of China. *Am. Assoc. Pet. Geol. Bull.* 83, 1004–1014. doi:10.1306/e4fd2e51-1732-11d7-8645000102c1865d

Chenet, P. Y., Colletta, B., Letouzey, J., Desforges, G., Ousset, E., and Zaghloul, E. A. (1987). Structures associated with extensional tectonics in the Suez rift. *Geol. Soc. Lond. Spec. Publ.* 28, 551–558. doi:10.1144/gsl.sp.1987.028.01.36

Coleman, R., and Billington, D. (1979). Membrane composition affects characteristics of glycocholate-induced lysis of erythrocytes. *Biochem. Soc. Trans.* 7 (5), 948. doi:10.1042/bst0070948

Delpino, D. H., and Bermúdez, A. M. (2009). Petroleum systems including unconventional reservoirs in intrusive igneous rocks (sills and laccoliths). *Lead. Edge* 28, 804–811. doi:10.1190/1.3167782

Dershowitz, W. S., and Herda, H. H. (1992). "Interpretation of fracture spacing and intensity," in *ARMA US rock mechanics/geomechanics symposium*. ARMA–92.

Elmaadawy, K. G., Bayan, M. F., and El-Shayeb, H. M. (2021). Source rock maturity and hydrocarbon potential of Abu Rudeis-Sidri area, central province, Gulf of Suez, Egypt. *Arab. J. Geosci.* 14, 2813–2817. doi:10.1007/s12517-021-09140-6

El Nady, M. M., and Mohamed, N. S. (2016). Source rock evaluation for hydrocarbon generation in Halal oilfield, southern Gulf of Suez, Egypt. *Egypt. J. Pet.* 25, 383–389. doi:10.1016/j.ejpe.2015.09.003

Endress, C., Furman, T., El-Rus, M. A. A., and Hanan, B. B. (2011). Geochemistry of 24 Ma basalts from NE Egypt: source components and fractionation history. *Geol. Soc. Lond. Spec. Publ.* 357, 265–283. doi:10.1144/sp357.14

Farouk, S., Sen, S., Belal, N., Omran, M. A., Assal, E. M., and Sarhan, M. A. (2023). Assessment of the petrophysical properties and hydrocarbon potential of the lower Miocene Nukhul Formation in the Abu rudeis-sidri field, gulf of suez basin, Egypt. *Geomech. Geophys. Geo-Energy Geo-Resources* 9, 36. doi:10.1007/s40948-023-00572-w

Fjeldskaar, W., Helset, H. M., Johansen, H., Grunnaleite, I., and Horstad, I. (2008). Thermal modelling of magmatic intrusions in the Gjallar Ridge, Norwegian Sea: implications for vitrinite reflectance and hydrocarbon maturation. *Basin Res.* 20, 143–159. doi:10.1111/j.1365-2117.2007.00347.x

Galushkin, Y. I. (1997). Thermal effects of igneous intrusions on maturity of organic matter: a possible mechanism of intrusion. *Org. Geochem.* 26, 645–658. doi:10.1016/s0146-6380(97)00030-2

Garfunkel, Z., Bartov, J., Eyal, Y., and Steinitz, G. (1974). Raham conglomerate – new evidence for Neogene tectonism in the southern part of the dead Sea rift. *Geol. Mag.* 111, 55–64. doi:10.1017/s0016756800000455

Geomatica (2017). *PCI Geomatica*.

Ghorab, M. A. (1961). "Abnormal stratigraphic features in Ras Gharib oil field," in *3rd arab petrol. Cong. Alexandria II*.

Grobe, A., Littke, R., Sachse, V., and Leythaeuser, D. (2015). Burial history and thermal maturity of Mesozoic rocks of the Dolomites, Northern Italy. *Swiss J. Geosci.* 108, 253–271. doi:10.1007/s00015-015-0191-2

Healy, D., Rizzo, R. E., Cornwell, D. G., Farrell, N. J. C., Watkins, H., Timms, N. E., et al. (2017). FracPaQ: a MATLAB™ toolbox for the quantification of fracture patterns. *J. Struct. Geol.* 95, 1–16. doi:10.1016/j.jsg.2016.12.003

Hegazi, A. M. (1995). *Structural analysis and metamorphic evolution of east Abu zeneima area*. Sinai: bibtex.txt.

Hewaidy, A. G. A., Farouk, S., and Ayyad, H. M. (2012). Nukhul formation in wadi baba, southwest sinai peninsula,Egypt. *GeoArabia* 17, 103–120. doi:10.2113/geoarabia1701103

Hewaidy, A. G. A., Farouk, S., and Ayyad, H. M. (2013). Foraminifera and sequence stratigraphy of Burdigalian - serravallian successions on the eastern side of the Gulf of Suez, southwestern Sinai, Egypt. *Neues Jahrb. fur Geol. Palaontologie - Abh.* 270, 151–170. doi:10.1127/0077-7749/2013/0362

Holford, S. P., Schofield, N., Jackson, C. A. L., Magee, C., Green, P. F., Duddy, I. R., et al. (2013). "Impacts of igneous intrusions on source and reservoir potential in prospective sedimentary basins along the western Australian continental margin," in *West Australian basins symposium*, 18–21.

Hubred, J. H. (2006). *Thermal effects of basaltic sill emplacement in source rocks on maturation and hydrocarbon generation*.

Hughes, G. W., Abdine, S., and Girgis, M. H. (1992). Miocene biofacies development and geological history of the Gulf of Suez, Egypt. *Mar. Pet. Geol.* 9, 2–28. doi:10.1016/0264-8172(92)90002-v

Kazmin, V. G., and Byakov, A. F. (2000). Magmatism and crustal accretion in continental rifts. *J. Afr. Earth Sci.* 30, 555–568. doi:10.1016/s0899-5362(00)00038-5

Khedr, F. I. (2003). *Structural studies on the northeastern sector of the Gulf of Suez*. Egypt.

Lee, E. Y., Tejada, M. L. G., Song, I., Chun, S. S., Gier, S., Riquier, L., et al. (2021). Petrophysical property modifications by alteration in a volcanic sequence at IODP

site U1513, naturaliste plateau. *J. Geophys. Res. Solid Earth* 126. doi:10.1029/2020JB021061

Manzocchi, T. (2002). The connectivity of two-dimensional networks of spatially correlated fractures. *Water Resour. Res.* 38, 1. doi:10.1029/2000wr000180

Mart, Y., and Hall, J. K. (1984). Structural trends in the northern Red Sea. *J. Geophys. Res.* 89, 11352–11364. doi:10.1029/jb089ib13p11352

Meneisy, M. Y. (1990). "Volcanicity," in *The Geology of Egypt*. Editor R. Said (Rotterdam, Netherlands: Balkema Pub), 157–172.

Mousa, H. E. (1987). *Geologic studies and genetic correlation of basaltic rocks in west central Sinai*. Ph. D thesis, Fac. Sci. Egypt: Ain Shams Univ.

Moustafa, A. R. (1993). Structural characteristics and tectonic evolution of the east-margin blocks of the Suez rift. *Tectonophysics* 223, 381–399. doi:10.1016/0040-1951(93)90146-b

Moustafa, A. R. (2004). *Geological maps of the eastern side of the Suez rift (western Sinai peninsula)*. Egypt: AAPG/Datapages.

Muirhead, D. K., Bowden, S. A., Parnell, J., and Schofield, N. (2017). Source rock maturation owing to igneous intrusion in rifted margin petroleum systems. *J. Geol. Soc. Lond.* 174, 979–987. doi:10.1144/jgs2017-011

Muirhead, D. K., Duffy, M., Schofield, N., Mark, N., and Rowe, M. D. (2020). Making oil from magma. *Geol. Soc. Lond. Spec. Publ.* 484, 295–303. doi:10.1144/sp484.8

Navelot, V., Géraud, Y., Favier, A., Diraison, M., Corsini, M., Lardeaux, J.-M., et al. (2018). Petrophysical properties of volcanic rocks and impacts of hydrothermal alteration in the Guadeloupe Archipelago (West Indies). *J. Volcanol. Geotherm. Res.* 360, 1–21. doi:10.1016/j.jvolgeores.2018.07.004

Othman, R., Arouri, K. R., Ward, C. R., and McKirdy, D. M. (2001). Oil generation by igneous intrusions in the northern Gunnedah Basin, Australia. *Org. Geochem.* 32, 1219–1232. doi:10.1016/s0146-6380(01)00089-4

Palumbo, F., Main, I. G., and Zito, G. (1999). The thermal evolution of sedimentary basins and its effect on the maturation of hydrocarbons. *Geophys. J. Int.* 139, 248–260. doi:10.1046/j.1365-246x.1999.00877.x

Patton, T. L., Moustafa, A. R., Nelson, R. A., and Abdine, S. A. (1994). *Tectonic evolution and structural setting of the Suez rift: chapter 1: Part I. Type basin: Gulf of Suez*.

Peace, A., McCaffrey, K., Imber, J., Hobbs, R., van Hunen, J., and Gerdes, K. (2017). Quantifying the influence of sill intrusion on the thermal evolution of organic-rich sedimentary rocks in nonvolcanic passive margins: an example from ODP 210-1276, offshore Newfoundland, Canada. *Basin Res.* 29, 249–265. doi:10.1111/bre.12131

Pepper, A. S., and Corvi, P. J. (1995). Simple kinetic models of petroleum formation. Part I: oil and gas generation from kerogen. *Mar. Pet. Geol.* 12, 291–319. doi:10.1016/0264-8172(95)98381-e

Plaziat, J.-C., Montenat, C., Barrier, P., Janin, M.-C., Orszag-Sperber, F., and Philobbos, E. (1998). Stratigraphy of the Egyptian syn-rift deposits: correlations between axial and peripheral sequences of the north-western Red Sea and Gulf of Suez and their relations with tectonics and eustacy. *Sediment. Tect. Rift. Basins Red. Sea-Gulf Aden* 1998, 211–222. doi:10.1007/978-94-011-4930-3_13

Ragab, A. I., and El-Kaliouby, B. A. (1992). Geodynamic of the Gulf of Suez-Red Sea rifting and origin of within plate magmatism. *J. Afr. Earth Sci. Middle East* 14, 351–360. doi:10.1016/0899-5362(92)90038-e

Reeckmann, S. A., and Mebberson, A. J. (1984). *Igneous intrusions in the north-west Canning Basin and their impact on oil exploration*.

Roberts, L. N. R., Finn, T. M., Lewan, M. D., and Kirschbaum, M. A. (2007). *Burial history, thermal maturity, and oil and gas generation history of petroleum systems in the Wind River Basin province, central Wyoming*. Reston, Virginia: US Geol. Surv., 30.

Robson, D. A. (1971). The structure of the Gulf of Suez (Clysmic) rift, with special reference to the eastern side. *J. Geol. Soc. Lond.* 127, 247–271. doi:10.1144/gsjgs.127.3.0247

Said, R. (1960). Planktonic foraminifera from the Thebes Formation, luxor, Egypt. *Micropaleontology* 6, 277–286. doi:10.2307/1484234

Said, R. (1962). *The geology of Egypt*. Amsterdam, New York: Springer.

Said, R. (1990). *The geology of Egypt: balkema*. Rotterdam, Brookf: Scientific Research Publishing, 734.

Salah, M. G. (1992). "Geochemical evaluation of the southern gulf of suez, Egypt," in *11th petroleum exploration and production conference* (Cairo), 383–395.

Schofield, N., Holford, S., Millett, J., Brown, D., Jolley, D., Passey, S. R., et al. (2017). Regional magma plumbing and emplacement mechanisms of the Faroe-Shetland Sill Complex: implications for magma transport and petroleum systems within sedimentary basins. *Basin Res.* 29, 41–63. doi:10.1111/bre.12164

Schutter, S. R. (2003a). Hydrocarbon occurrence and exploration in and around igneous rocks. *Geol. Soc. Lond. Spec. Publ.* 214, 7–33. doi:10.1144/gsl.sp.2003.214.01.02

Schutter, S. R. (2003b). Occurrences of hydrocarbons in and around igneous rocks. *Geol. Soc. Lond. Spec. Publ.* 214, 35–68. doi:10.1144/gsl.sp.2003.214.01.03

Scott, R. W., and Govean, F. M. (1985). Early depositional history of a rift basin: Miocene in Western Sinai. *Palaeogeogr. Palaeoclimatol. Palaeoecol.* 52, 143–158. doi:10.1016/0031-0182(85)90035-5

Seleem, T. A., and Khalifa, I. H. (2006). Structural control of sulphide mineralization in wadi el-rusis and wadi remthi localities, south sinai, Egypt. *Magallat al-"Ulum al-Giyulugiyyat li-l-Gumhuriyyat al-"Arabiyyat al-Muttahidat/United Arab. Repub. J. Geol.* 50, 289.

Shallaly, N. A., Beier, C., Haase, K. M., and Hammed, M. S. (2013). Petrology and geochemistry of the tertiary Suez rift volcanism, sinai, Egypt. *J. Volcanol. Geotherm. Res.* 267, 119–137. doi:10.1016/j.jvolgeores.2013.10.005

Sharib, A. S. A. A. A., Selim, A. Q., Fattah, M. M. A., Hassan, S. M., and Sanislav, I. V. (2019). Thermal alteration of organic matter in the contact of a rift-related basaltic dyke: an example from the black limestone,wadi matulla,west central sinai, Egypt. *Minerals* 9, 279. doi:10.3390/min9050279

Simandl, G. J., Paradis, S., and Akam, C. (2015). Graphite deposit types, their origin, and economic significance. *Br. Columbia Minist. Energy Mines \and Br. Columbia Geol. Surv.* 3, 163–171.

Steen, G. (1982). "Radiometric age dating and tectonic significance of some Gulf of Suez igneous rocks," in *6th petrol. Explor. Seminar*.

Stewart, A. K., Massey, M., Padgett, P. L., Rimmer, S. M., and Hower, J. C. (2005). Influence of a basic intrusion on the vitrinite reflectance and chemistry of the Springfield (No. 5) coal, Harrisburg, Illinois. *Int. J. Coal Geol.* 63, 58–67. doi:10.1016/j.coal.2005.02.005

Suzuki, N., Matsubayashi, H., and Waples, D. W. (1993). A simpler kinetic model of vitrinite reflectance. *Am. Assoc. Pet. Geol. Bull.* 77. doi:10.1306/bdff8eca-1718-11d7-8645000102c1865d

Sydnes, M., Fjeldskaar, W., Løtveit, I. F., Grunnaleite, I., and Cardozo, N. (2018). The importance of sill thickness and timing of sill emplacement on hydrocarbon maturation. *Mar. Pet. Geol.* 89, 500–514. doi:10.1016/j.marpetgeo.2017.10.017

Vásquez, M., Altenberger, U., and Romer, R. L. (2009). Neogene magmatism and its possible causal relationship with hydrocarbon generation in SW Colombia. *Int. J. Earth Sci.* 98, 1053–1062. doi:10.1007/s00531-008-0303-6

Wang, D., Lu, X., Zhang, X., Xu, S., Hu, W., and Wang, L. (2007). Heat-model analysis of wall rocks below a diabase sill in Huimin Sag, China compared with thermal alteration of mudstone to carbargilite and hornfels and with increase of vitrinite reflectance. *Geophys. Res. Lett.* 34. doi:10.1029/2007gl030314

Wang, D., Song, Y., Xu, H., Ma, X., and Zhao, M. (2013). Numerical modeling of thermal evolution in the contact aureole of a 0.9 m thick dolerite dike in the Jurassic siltstone section from Isle of Skye, Scotland. *J. Appl. Geophys.* 89, 134–140. doi:10.1016/j.jappgeo.2012.12.004

Wang, D., Zhao, M., and Qi, T. (2012). Heat-transfer-model analysis of the thermal effect of intrusive sills on organic-rich host rocks in sedimentary basins. *Earth Sci.* 5, 92–98.

Wever, H. E. (1999). A common source rock for Egyptian and Saudi hydrocarbons in the Red Sea: discussion. *Am. Assoc. Pet. Geol. Bull.* 83, 802–804. doi:10.1306/e4fd2d93-1732-11d7-8645000102c1865d

Witte, J., Bonora, M., Carbone, C., and Oncken, O. (2012). Fracture evolution in oil-producing sills of the rio grande valley, northern neuquén basin, Argentina. *Am. Assoc. Pet. Geol. Bull.* 96, 1253–1277. doi:10.1306/10181110152

Wu, C., Gu, L., Zhang, Z., Ren, Z., Chen, Z., and Li, W. (2006). Formation mechanisms of hydrocarbon reservoirs associated with volcanic and subvolcanic intrusive rocks: examples in Mesozoic--Cenozoic basins of eastern China. *Am. Assoc. Pet. Geol. Bull.* 90, 137–147. doi:10.1306/04070505004

Yiming, A., Bian, B., Liu, H., Wang, J., Wang, X., Zhu, J., et al. (2023). Development characteristics and main controlling factors of Carboniferous volcanic reservoirs in the Shixi area, Junggar Basin. *Front. Earth Sci.* 11, 1–13. doi:10.3389/feart.2023.1185213

Younes, M. A., and Philp, R. P. (2005). Source rock characterization based on biological marker distributions of crude oils in the southern gulf of suez, Egypt. *J. Pet. Geol.* 28, 301–317. doi:10.1111/j.1747-5457.2005.tb00085.x

Youssef, M. I. (1949). *Stratigraphical studies in Qusseir area*. Ph. D. Thesis. Egypt: Alexandria Univ.

Youssef, M. I. (1957). Upper cretaceous rocks in quesir area. *Bull. L'Institute Egypt* 7, 35–63.

Zalat, A. A., Zaid, S. M., Gadallah, M. H., and Abdel-Aziz, Z. A. (2012). Sandstones reservoir quality of the Matulla Formation, gulf of suez, Egypt. *Aust. J. Basic Appl. Sci.* 6, 511–529.

Zhu, D., Jin, Z., Hu, W., Song, Y., and Gao, X. (2007). Effect of igneous activity on hydrocarbon source rocks in Jiyang sub-basin, eastern China. *J. Pet. Sci. Eng.* 59, 309–320. doi:10.1016/j.petrol.2007.05.002